

NUWC-NPT Technical Document 10,172
1 March 1993

AD-A263 733



2

Design and Analysis of an Apparatus for Measuring the Drag Coefficients of Flexible Wire Cable

J. R. Milburn
Launcher and Missile Systems Department

DTIC
ELECTE
MAY 05 1993
S B D



**Naval Undersea Warfare Center Division
Newport, Rhode Island**

Original contains color
plates. All DTIC reproductions
will be in black and
white.

Approved for public release; distribution is unlimited.

93-09617 80pb

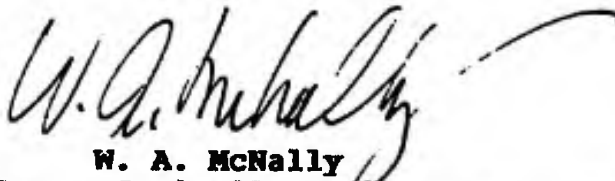
93 5 04 15 8

PREFACE

This document is a modified version of the author's URI masters thesis, which was originally completed and published in 1992. Some minor editing and reformatting of the original thesis have been done. The work described was partially funded by the Naval Undersea Warfare Center (NUWC) Division, Newport, RI, and is pertinent to NUWC's Improved Flex-Hose Project.

The author would like to thank Dr. Philip Datseris of URI for his technical guidance, and Mr. John Babb of NUWC for his advice and support throughout this project.

Reviewed and Approved: 1 March 1993

A handwritten signature in black ink, appearing to read "W. A. McNally", with a long, sweeping flourish extending to the right.

W. A. McNally
Head, Launcher and Missile Systems Department

DISCLAIMER NOTICE



THIS DOCUMENT IS BEST QUALITY AVAILABLE. THE COPY FURNISHED TO DTIC CONTAINED A SIGNIFICANT NUMBER OF COLOR PAGES WHICH DO NOT REPRODUCE LEGIBLY ON BLACK AND WHITE MICROFICHE.

REPORT DOCUMENTATION PAGEForm Approved
OMB No. 0704-0188

Public reporting burden for this collection of information is estimated to average 1 hour per response, including the time for reviewing instructions, searching existing data sources, gathering and maintaining the data needed, and completing and reviewing the collection of information. Send comments regarding this burden estimate or any other aspect of this collection of information, including suggestions for reducing this burden, to Washington Headquarters Services, Directorate for Information Operations and Reports, 1215 Jefferson Davis Highway, Suite 1204, Arlington, VA 22202-4302, and to the Office of Management and Budget, Paperwork Reduction Project (0704-0188), Washington, DC 20303.

1. AGENCY USE ONLY (Leave blank)		2. REPORT DATE 1 March 1993	3. REPORT TYPE AND DATES COVERED	
4. TITLE AND SUBTITLE Design and Analysis of an Apparatus for Measuring the Drag Coefficients of Flexible Wire Cable			5. FUNDING NUMBERS	
6. AUTHOR(S) J. R. Milburn			7. PERFORMING ORGANIZATION NAME(S) AND ADDRESS(ES) Naval Undersea Warfare Center Division Newport, RI 02841-1708	
7. PERFORMING ORGANIZATION NAME(S) AND ADDRESS(ES) Naval Undersea Warfare Center Division Newport, RI 02841-1708			8. PERFORMING ORGANIZATION REPORT NUMBER TD 10,172	
9. SPONSORING/MONITORING AGENCY NAME(S) AND ADDRESS(ES)			10. SPONSORING/MONITORING AGENCY REPORT NUMBER	
11. SUPPLEMENTARY NOTES A thesis submitted in partial fulfillment of the requirements for the degree of Master of Science in Mechanical Engineering, University of Rhode Island, 1992.				
12a. DISTRIBUTION/AVAILABILITY STATEMENT Approved for public release; distribution is unlimited.			12b. DISTRIBUTION CODE	
13. ABSTRACT (Maximum 200 words) A novel design of a two-point attachment apparatus for measuring normal and tangential drag coefficients of a flexible wire conduit is presented. A technique is developed to stiffen the flexible cable so that its catenary is reduced. An instrumentation method that accurately measures the desired in-line forces is also presented. The fundamental frequencies of vibration are calculated for the drag apparatus and compared with the expected excitation forces.				
14. SUBJECT TERMS Hydrodynamics Drag Coefficients Drag Forces Mechanical Cables			15. NUMBER OF PAGES 80	
			16. PRICE CODE	
17. SECURITY CLASSIFICATION OF REPORT UNCLASSIFIED	18. SECURITY CLASSIFICATION OF THIS PAGE UNCLASSIFIED	19. SECURITY CLASSIFICATION OF ABSTRACT UNCLASSIFIED	20. LIMITATION OF ABSTRACT SAR	

TABLE OF CONTENTS

Chapter		Page
	LIST OF FIGURES.....	iii
	NOMENCLATURE.....	v
1	EXPERIMENTAL TECHNIQUE.....	1
	1.1 Introduction.....	1
	1.2 Previous Work.....	3
	1.3 Governing Equations.....	4
	1.4 Comparison of Previous Work and Its Uncertainty... 10	
	1.5 Design Methodology.....	17
2	DRAG APPARATUS TEST SECTION.....	19
	2.1 Description of Test Section.....	19
	2.2 Fixed-End Condition.....	21
	2.3 Simply Supported Condition.....	30
	2.4 Test Section Design.....	35
3	INSTRUMENTATION.....	37
	3.1 Transducer Setup.....	37
	3.2 Simply Supported Case.....	38
	3.3 Fixed-End Condition.....	41
	3.4 Comparison of the End Conditions.....	59

TABLE OF CONTENTS (Cont'd)

Chapter	Page
4 VIBRATION ANALYSIS.....	61
4.1 Introduction.....	61
4.2 Eigenvalue Extraction.....	61
4.3 Vortex Shedding.....	71
4.4 Comparison of FEM and Calculated Values.....	73
4.5 Vibration Considerations.....	74
 5 SUMMARY AND CONCLUSIONS.....	 77
 REFERENCES.....	 81
BIBLIOGRAPHY.....	83

Accession For

NTIS GRA&I

DTIC TAB

Unannounced

Justification

By

Distribution/

Availability Codes

Dist	Avail and/or Special
A-1	

DTIC QUALITY INSPECTED 8

LIST OF FIGURES

Figure	Page
1.1 Torpedo Launch Cycle.....	2
1.2 Free Body Diagram.....	6
1.3 Normal Drag Coefficient vs Tow Angle.....	11
1.4 Normal Drag Coefficient vs Tow Angle.....	12
1.5 Uncertainty in the Normal Drag Coefficient +/- 0.5 Deg.	15
1.6 Uncertainty in the Normal Drag Coefficient +/- 1.0 Deg.	16
1.7 Drag Apparatus.....	18
2.1 Test Section Orientation.....	20
2.2 Fixed-End Condition.....	21
2.3 End Moment vs Tension at Fixed End.....	27
2.4 Mid-Point Deflection vs Tension at Fixed End.....	28
2.5 Von Mises Stress vs Tension at Fixed End.....	29
2.6 Simply Supported Condition.....	30
2.7 Von Mises Stress vs Tension, Simply Supported.....	33
2.8 Mid-Point Deflection vs Tension, Simply Supported.....	34
3.1 Simply Supported Transducer.....	40
3.2 Fixed-End Transducer.....	42
3.3 Mesh of Transducer.....	45
3.4 Deflection of Transducer.....	47
3.5 Von Mises Stress, Bird's Eye View.....	49

LIST OF FIGURES (Cont'd)

Figure	Page
3.6 Von Mises Stress, Back View.....	51
3.7 Von Mises Stress, Top View.....	53
3.8 Von Mises Stress, Front View.....	55
3.9 Von Mises Stress, Deflected.....	57
4.1 Beam Model of Drag Apparatus.....	62
4.2 Test Section Fundamental Mode.....	65
4.3 Vertical Strut Fundamental Mode.....	67
4.4 Vertical Strut Second Fundamental.....	69

NOMENCLATURE

Chapter 1:

F	Tangential Force Acting on Cable
T	In-Line Tension Acting on Cable
N	Normal Force Acting on Cable
W	Cable Weight per Unit Length
θ	Cable Angle with Respect to Flow
D	Diameter of Cable
C_{dt}	Tangential Drag Coefficient
ρ	Density of Water
V_t	Tangential Velocity
$Q(\theta)$	Change in Normal Force on Element of Cable
R	Force Acting on Cable at 90 Degrees to Flow
V_n	Normal Velocity
C_{dn}	Normal Drag Coefficient
C_{dl}	Lift Coefficient
Ψ	Kite Angle of Cable

Chapter 2:

W	Drag Load Per Unit Length
M_o	End Moment
T	In-Line Tension
E	Young's Modulus
I	Moment Area of Inertia

V_o	Shear Force
X	Displacement in X Direction
Y	Displacement in Y Direction
σ	Component of Stress
A	Cross Sectional Area
c	Distance to Neutral axis
τ	Shear Stress

CHAPTER 1: EXPERIMENTAL TECHNIQUE

1.1 INTRODUCTION

The Naval Undersea Warfare Center Division, Newport, Rhode Island, has been developing a computer code to simulate the dynamic behavior of flexible hose deployment during the launch cycle of wire guided torpedoes, Figure 1.1. The accuracy of this computer code is highly dependent on the accuracies of the hydrodynamic loading functions on the cable. A number of experiments have been performed on various types of flexible conduit to determine the hydrodynamic drag coefficients. Typically, these experiments were performed by towing sections of cable while measuring the tow point tension and the tow angle. With this information, it is possible to obtain the hydrodynamic drag coefficients of the cable. It will be shown that at higher speeds and small tow angles this approach leads to large inaccuracies in the drag coefficients. Further, during the deployment cycle of a wire guided device, the umbilical cable is forced into non-critical angle positions. Typically, the hydrodynamic loading functions for these cable configurations are derived from critical angle experiments.

As a result of the inaccuracies of the critical angle experiments and the application of critical angle data to non-critical angle configurations, an alternative approach is

FLEXIBLE HOSE DEPLOYMENT

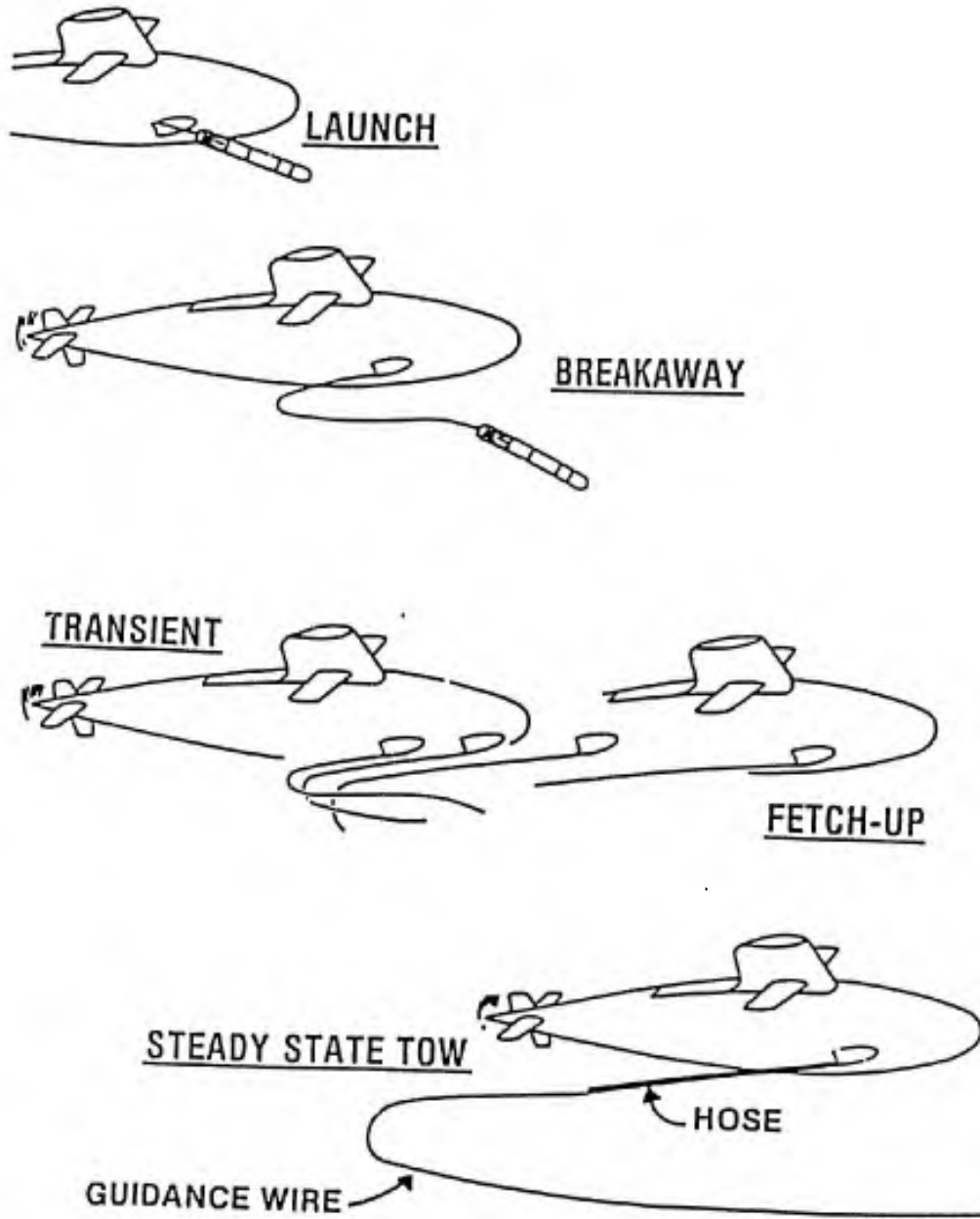


Figure 1.1. Torpedo Launch Cycle

designed. This approach consists of the development of an apparatus that measures the normal and tangential drag forces directly.

1.2 PREVIOUS WORK

Several past experimental efforts have attempted to determine the hydrodynamic forces that affect specific flexible cables in a uniform stream.

Pode, of the David Taylor Model Basin, tested several stranded cables (reference 1). The purpose of the work was to develop a relationship between the hydrodynamic forces acting on the cable and their critical tow angles.

Puryear and Gay, of the Naval Ship Research and Development Center, tested six different configurations of flexible conduit (reference 2). Each configuration was towed in a high speed tow basin to obtain data from which hydrodynamic loads could be determined.

Diggs, of the Naval Ship Research and Development Center, undertook a comprehensive program to develop the hydrodynamic technology of towed arrays (reference 3). This work included testing of various cables in a tow tank system and during at-sea evaluations.

Holler, of the Naval Air Development Center, conducted a series of at-sea tests on various suspended cables (reference 4). The tow point tension and tow angle were measured in an effort to determine hydrodynamic drag coefficients.

Babb, Hassan, and Labrecque, of the Naval Underwater Systems Center, conducted a series of experiments to determine the normal and tangential drag coefficients of several spirally wound flexible hoses (reference 5). These tests were performed at the University of Rhode Island Tow Tank Facility.

Babb, Milburn, and McGrath, of the Naval Underwater Systems Center, conducted a series of tests to determine the hydrodynamic drag coefficients of several flexible cables (reference 6). These tests were conducted at the NUSC/NASA Tow Tank Facility in Hampton, Virginia.

All of these experiments were performed at critical tow angles. Before results from these experiments are analyzed and compared, a system definition is required.

1.3 GOVERNING EQUATIONS

One of the first attempts to address the characteristics of a flexible cable in a uniform stream was completed by Pode in 1951 (reference 7). In an effort to create tables for computing the equilibrium configuration of a flexible cable, Pode solved the governing differential equations of a flexible cable system. These equations provided the basis of many experimental studies that followed; therefore, Pode's system definition will be used. Governing equations are rearranged and simplified in terms of the hydrodynamic drag coefficients as a function of easily measurable properties.

The forces that act on an element of cable have three basic components. The first is the hydrodynamic force, which stems from the flow; the second is the weight of the cable in the fluid; and the third is the tension in the cable at the ends of the element. It is assumed that the hydrodynamic force acts on an infinitely long cylinder and is similar in proportion to a small element inclined at the same angle. Considering figure 1.2, which shows an element of a cable having unit length ds , the summation of tangential forces yields

$$\frac{dT}{ds} - \frac{F \cos \theta}{|\cos \theta|} - W \sin \theta = 0 \quad (1.1)$$

where the three terms represent in-line tension, the tangential drag per unit length and the tangential weight component. The sign and the COS functions in the second term of equation (1.1) are proper in order to take into account the fact that the tangential component of the hydrodynamic force never has a positive projection in the direction of motion. Equation (1.1) can be manipulated to find the tangential drag coefficient:

$$F = \frac{1}{2} \rho V_t^2 D C_{dt} \quad (1.2)$$

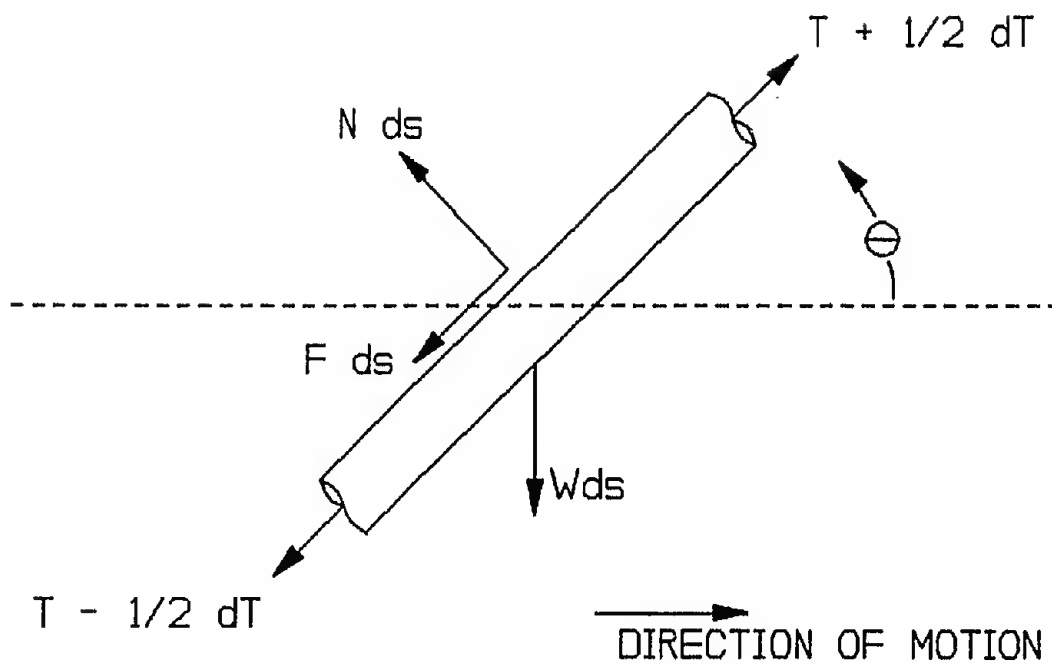


Figure 1.2. Free Body Diagram

thus,

$$C_{dt} = \frac{\frac{dT}{ds} - W \sin \theta}{\frac{1}{2} \rho V_t^2 D} \quad (1.3)$$

The normal force acting on an element of a cable can be shown to be equal to

$$N ds = R \sin(\theta) |\sin(\theta)| ds \quad (1.4)$$

where R is the normal force acting on the cable when the cable is 90 degrees to the flow.

Equation (1.4) is derived by resolving the horizontal normal force R. When multiplied by $\sin(\theta)$, R can be resolved so that it acts in a perpendicular fashion to the cable. If this term is then multiplied by the projected normal element length, $\sin(\theta) ds$, it gives the total normal force per unit length shown in equation (1.4).

The summation per unit length in the normal direction is given by

$$R \sin \theta |\sin \theta| - W \cos \theta = 0 \quad (1.5)$$

where the first term is the normal component of drag and the second term is the normal component of weight. The sign and the SIN functions in the first term of equation (1.5) are proper in order to take into account the fact that the normal component of the hydrodynamic force never has a positive projection in the direction of motion.

The normal component of the hydrodynamic force varies with the square of the sine of the angle between the cable and the stream. This is well established by experimental evidence and supported by theoretical considerations (reference 7).

Equation (1.5) can be manipulated to find the normal drag coefficient. The first step is to substitute

$$\sin^2\theta=1-\cos^2\theta \quad (1.6)$$

and divide by the normal force. Solving for the cosine of the cable angle gives

$$\cos\theta=-\frac{W}{2R}\pm\sqrt{\left(\frac{W}{2R}\right)^2+1} \quad (1.7)$$

where

$$R = \frac{1}{2} \rho V_n^2 D C_{dn} \quad (1.8)$$

and

$$C_{dn} = \frac{2W\cos\theta}{\rho V_n^2 D} \quad (1.9)$$

Examining these equations, one can readily see how these coefficients can be determined using a critical angle technique where the tow angle and the tow point tension are measured.

In 1974, Diggs (reference 3) expanded these equations to include one more dimension referred to as the kite angle. This assumes that the cable is wound asymmetrically, which in turn causes a circulation lift. This changes the tangential and normal components of drag and adds a third coefficient, lift. Diggs derives these coefficients to be

$$C_{dn} = \frac{W \cos \theta \cos \psi}{\frac{\rho}{2} DV_n^2 (1 + \cot^2 \theta \sin^2 \psi)^{\frac{3}{2}}} \quad (1.10)$$

$$C_{dt} = \frac{P(\theta) - W \sin \theta}{\frac{\rho}{2} DV_t^2 \cos^2 \psi} \quad (1.11)$$

$$C_{dl} = \frac{W \cot \theta \sin \psi}{\frac{\rho}{2} DV^2 (1 + \cot^2 \theta \sin^2 \psi)^{\frac{1}{2}}} \quad (1.12)$$

It is easily shown that when the kite angle is zero the lift coefficient is zero, and the normal and tangential drag terms reduce to Pote's equations. Using these equations, it is possible to compare much of the previous experimental work and assess its adequacy in the determination of these coefficients.

1.4 COMPARISON OF PREVIOUS WORK AND ITS UNCERTAINTY

Previous experiments that attempted to determine the hydrodynamic forces that affect specific cables typically measured the critical angle of tow, the tow point tension, the velocity of the tow point, and the weight of the cable. With this information and the equations above, it is possible to calculate the hydrodynamic drag coefficients. Plotting selected normal drag coefficients versus the angle of attack is enlightening.

Figure 1.3 shows an assortment of data from three separate tests carried out on the same cable by Babb in 1987 to 1989 (references 5 and 6). This figure indicates that as the tow angle decreases the calculated normal drag coefficient becomes uncertain. The author attributes this to the difficulty in the measurement of the tow angle when the cable is at small angles of attack.

Figure 1.4 shows the calculated normal drag coefficient vs the measured tow angles for various cables. This work was carried out by Diggs in 1974 (reference 3). Again, it is readily seen that as the cable angle decreases the calculated normal drag coefficient is inconsistent.

Although each author has his own interpretation of what data should be discarded, they all agree that the measurement of the tow angle when it has a small angle of attack is difficult. Puryear and Gay recommend that measured angles of

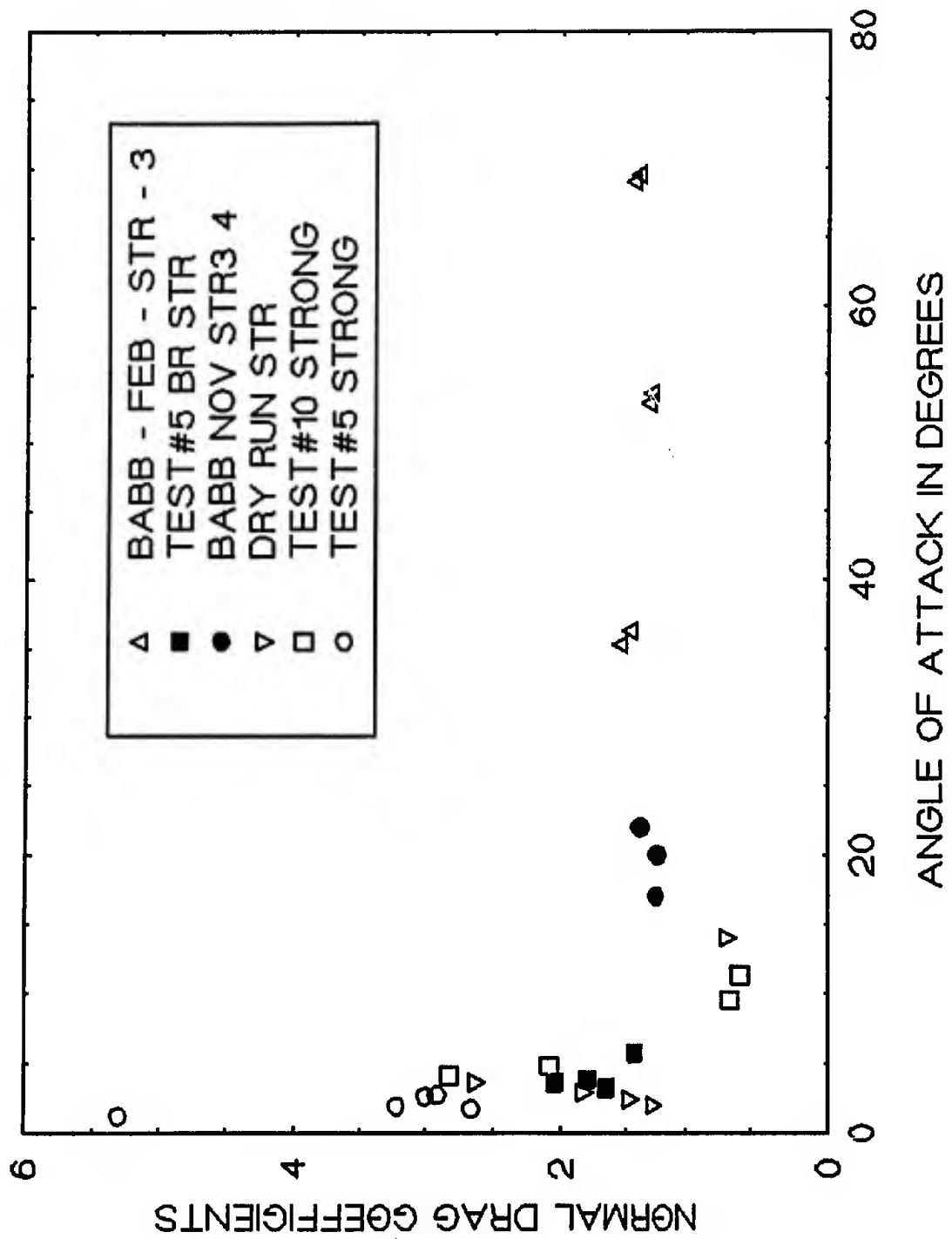


Figure 1.3. Normal Drag Coefficient vs Tow Angle

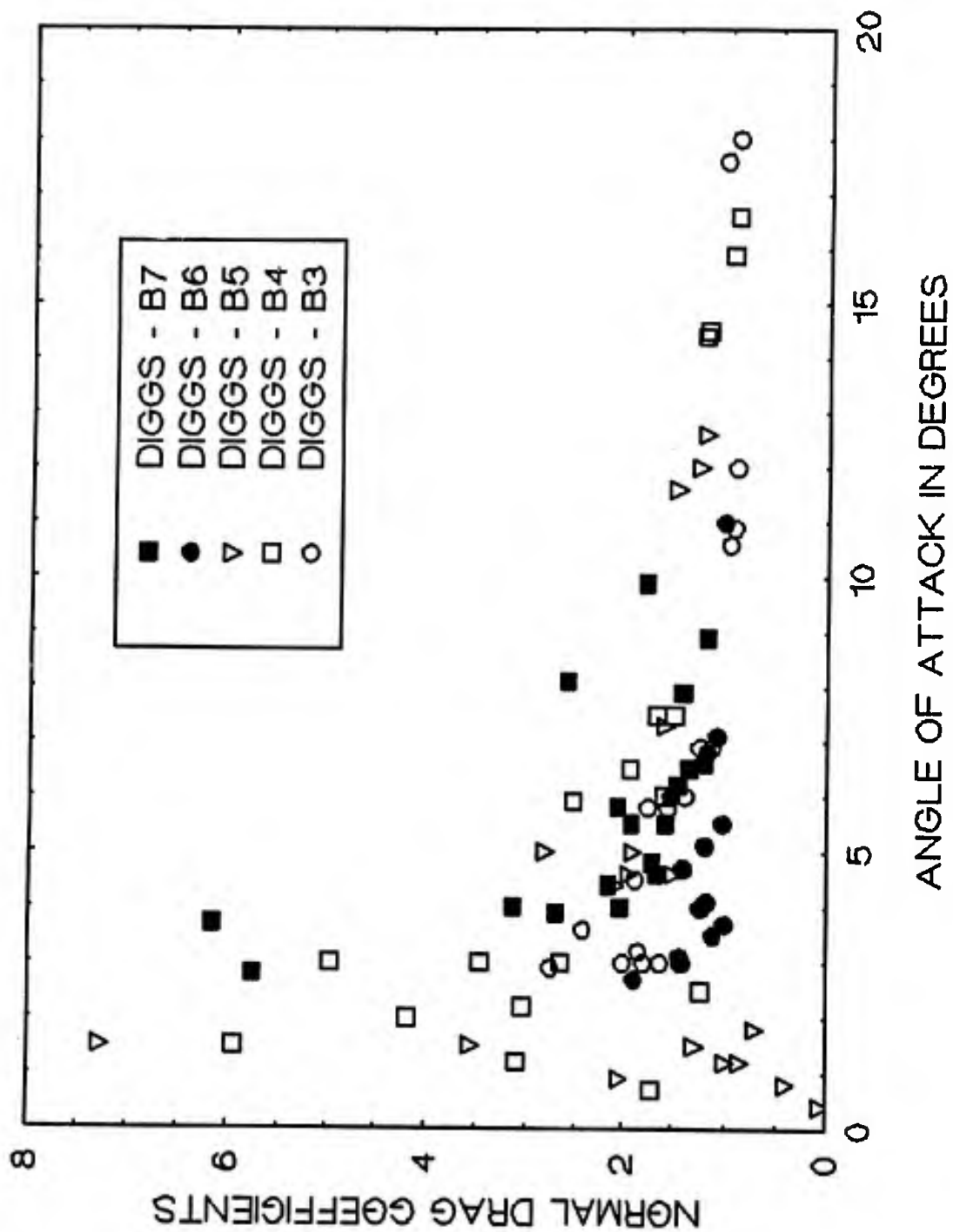


Figure 1.4. Normal Drag Coefficient vs Tow Angle

less than 5 degrees should be ignored (reference 2), whereas Babb, Milburn, and McGrath place a tolerance on their tow angles of plus or minus 0.5 degree (reference 6). This tolerance for small tow angle leads to significant percent error. It will be shown that the inherent inaccuracy of the measured tow angle at small angle of attack leads to large uncertainties in the calculated normal drag coefficient. In an effort to better explain this phenomenon a sensitivity analysis is presented.

Form equation (1.9) one can see that the normal drag coefficient is a function of velocity, density, diameter, weight, and the tow angle. Employing the uncertainty process developed by Kline and McClintock (reference 8), requires that the partial derivative of each of these variables be taken with respect to the normal drag coefficient. These derivatives are

$$\frac{\partial C_{dn}}{\partial W} = \frac{2 \cos \theta}{\sin^2 \theta \rho V^2 D} \quad (1.13)$$

$$\frac{\partial C_{dn}}{\partial D} = \frac{-2W \cos \theta}{\sin^2 \theta \rho V^2 D^2} \quad (1.14)$$

$$\frac{\partial C_{dn}}{\partial \rho} = \frac{-2W \cos \theta}{\sin^2 \theta \rho^2 V^2 D} \quad (1.15)$$

$$\frac{\partial C_{dn}}{\partial \theta} = \frac{-2W(\sin^3\theta + 2\sin\theta\cos^2\theta)}{\rho V^2 D \sin^4\theta} \quad (1.16)$$

$$\frac{\partial C_{dn}}{\partial V} = \frac{-4W(\cos^2\theta)}{\rho V^3 D \sin^2\theta} \quad (1.17)$$

The total uncertainty is computed by summing the squares of these partials, then taking their square root, which yields

$$U_{C_{dn}} = \sqrt{u_N(1.13)^2 + u_D(1.14)^2 + u_\rho(1.15)^2 + u_\theta(1.16)^2 + u_V(1.17)^2}.$$

A computer code was developed to determine the total uncertainty of the normal drag coefficient. The inputs to this code are simply the physical variables shown above.

Two plots illustrate clearly the uncertainty related to calculating the normal drag coefficient at small angles of attack. The first plot assumes that one can determine the tow angle to within 0.5 degree, and the second assumes that one can measure the tow angle to within 1.0 degree of the actual angle. A review of experimental work shows these to be conservative approximations.

The uncertainty shown in these graphs for small angles of attack is at best on the order of 400 to 500 percent. For this reason it is felt that a better methodology is required so that more realistic drag coefficients can be obtained.

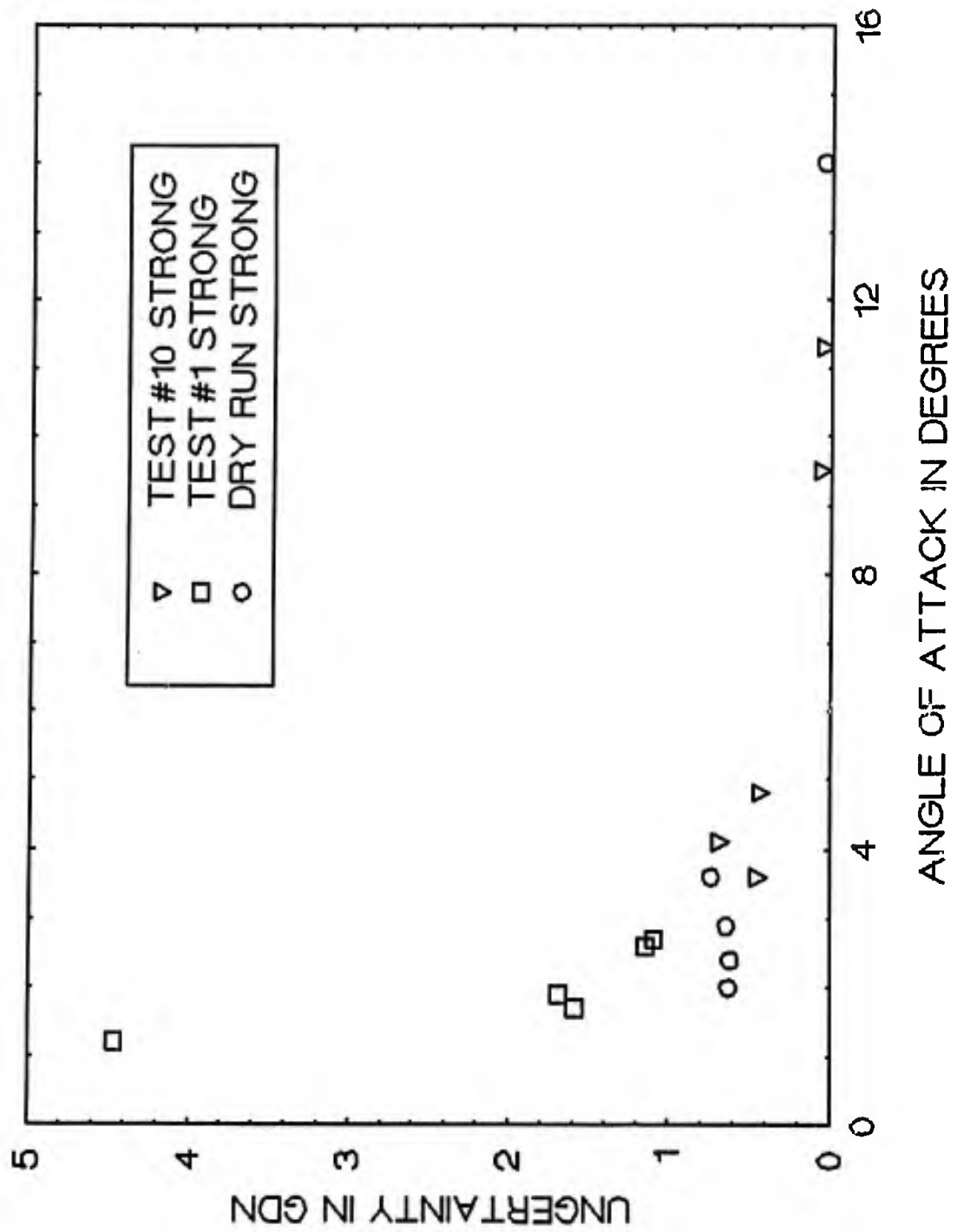


Figure 1.5. Uncertainty in the Normal Drag Coefficient +/- 0.5 Deg

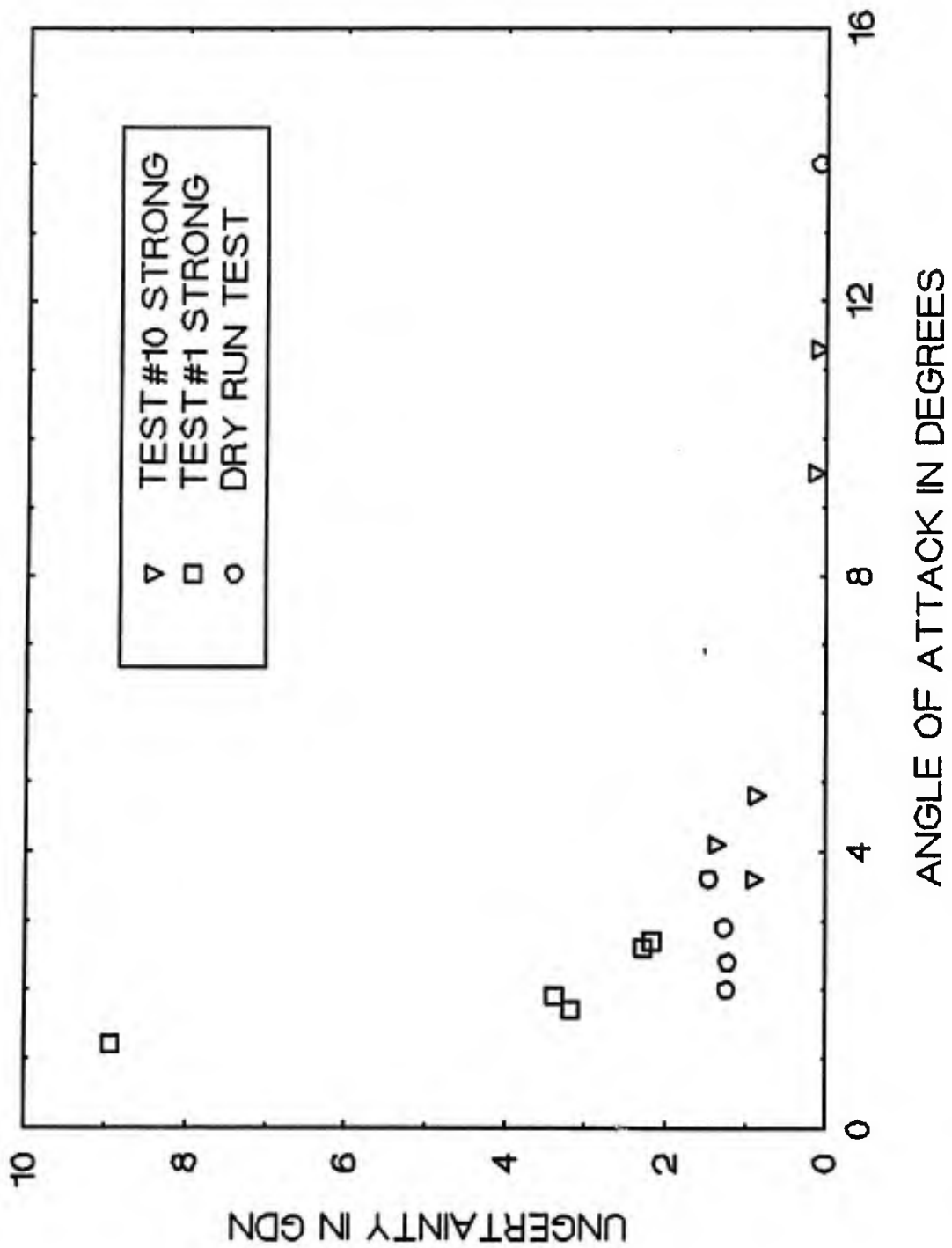


Figure 1.6. Uncertainty in the Normal Drag Coefficient +/- 1.0 Deg

1.5 DESIGN METHODOLOGY

Instead of using a critical tow angle technique, it is felt that a two-point drag apparatus would be better suited, figure 1.7. This apparatus has the ability to pull flexible cables at various angles of attack at speeds up to 20 knots. The test section has to sustain a catenary of less than 2 percent in order to maintain a specific angle of attack. This requires that the deflection at the center of the test section not exceed 2 percent of its total length. Biaxial force transducers are placed on each end of the test section so that the hydrodynamic loading can be measured directly. With this information it will be possible to compute the normal drag coefficients at high velocities at numerous angles of attack without having an inherent uncertainty in the tow angle.

The design of the two-point drag apparatus is accomplished in three succinct steps. First, a method is developed for stiffening the flexible cable so that the catenary is less than 2 percent of its total length. Second, an instrumentation method is developed that accurately measures normal and tangential forces on the cable. Finally, based on the constraints of the Langley Tow Tank Facility, the remaining conceptual design is completed and a vibration analysis is performed.

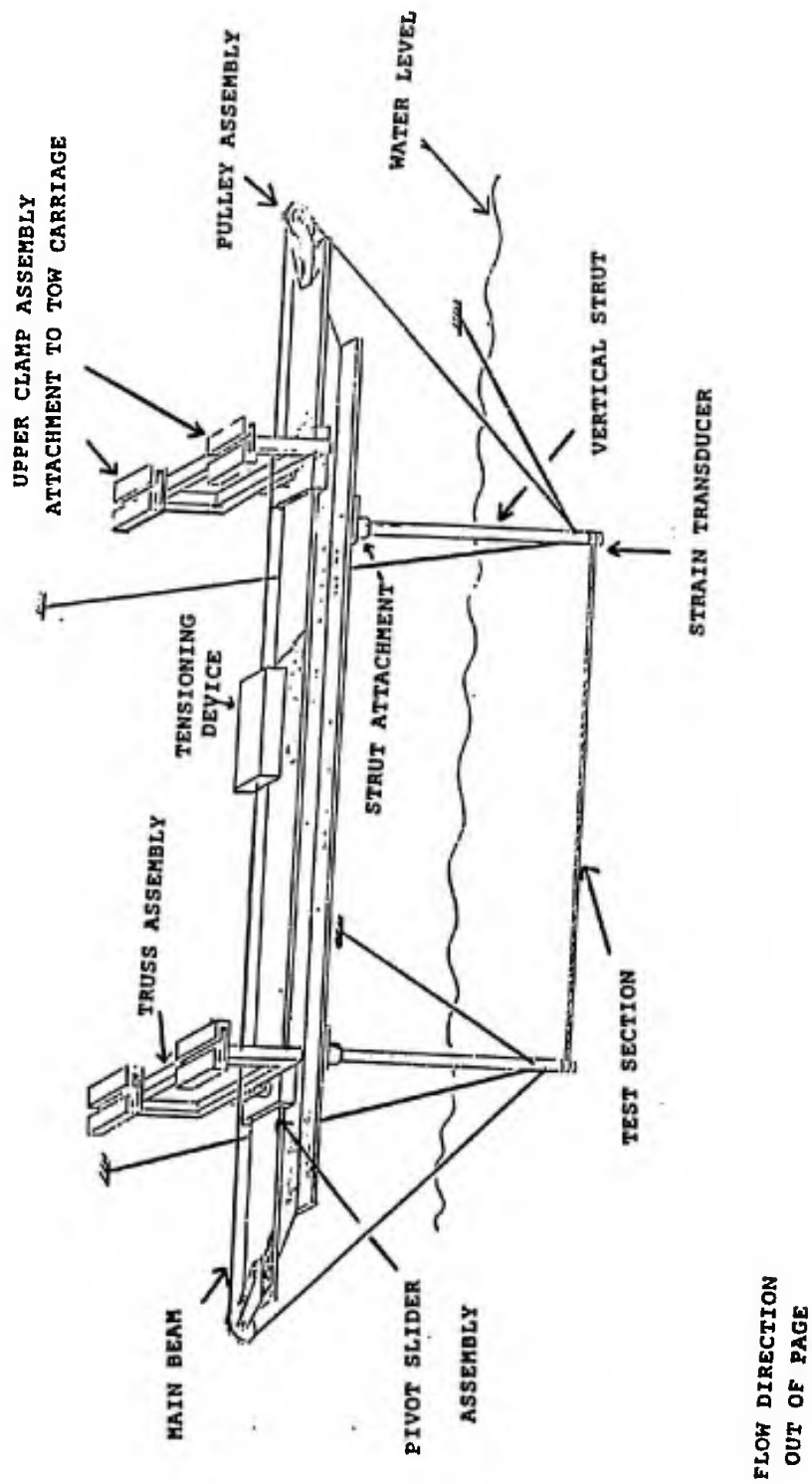


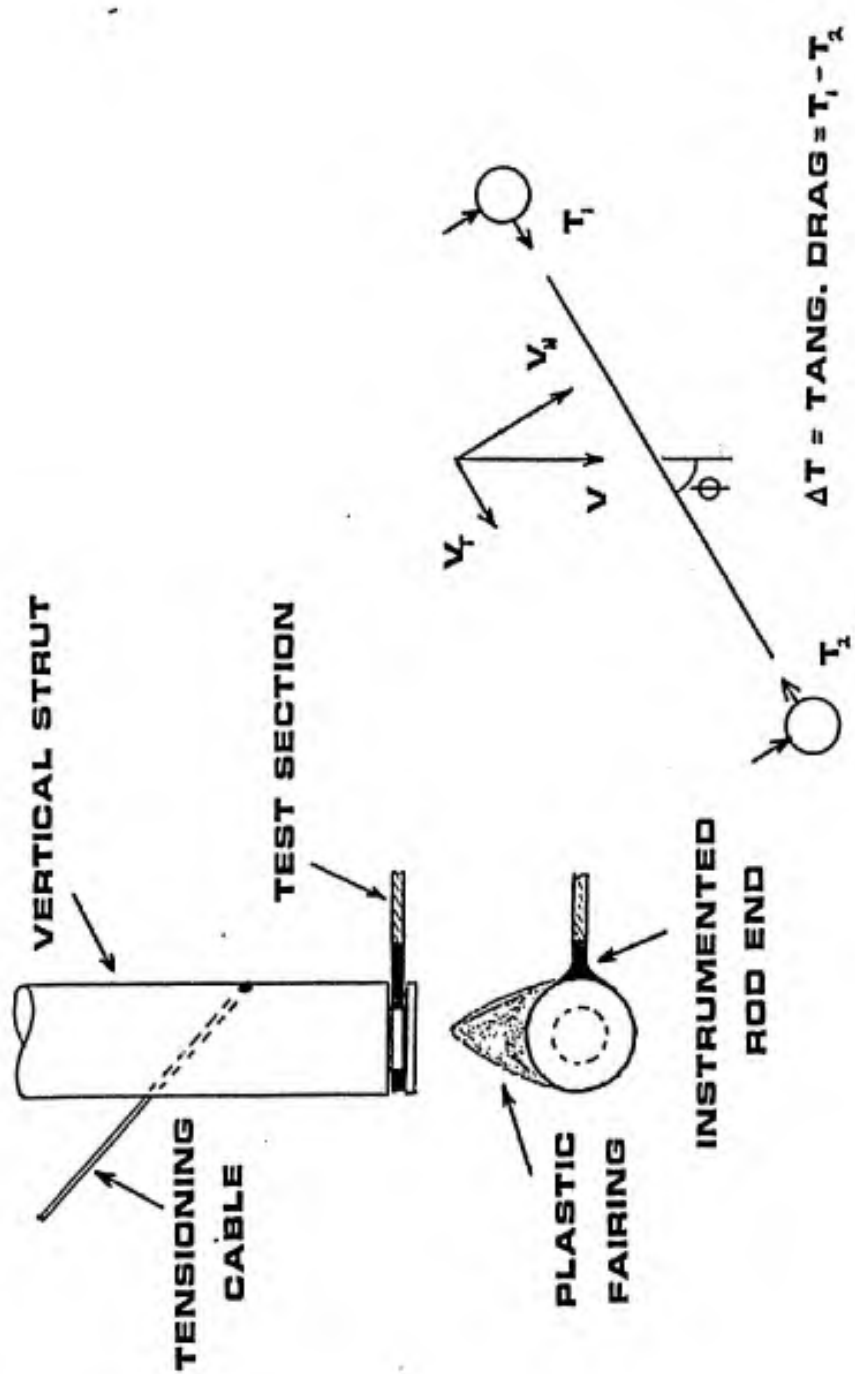
Figure 1.7. Drag Apparatus

CHAPTER 2: DRAG APPARATUS TEST SECTION

2.1 DESCRIPTION OF THE TEST SECTION

A drag apparatus that utilizes a test section attached at both ends was described conceptually in chapter 1, figure 1.7. The test section of this apparatus will be the focus of this chapter. It is required that the test section's catenary be as small as possible. This will insure that the in-line tension forces can be discerned from the perpendicular forces because each portion of the test section will be inclined at the same angle with respect to the flow. The test section will be supported on both ends as shown in figure 2.1. As a design goal the maximum center deflection is required to be less than 2 percent of the total length. In an effort to reduce the catenary of the test section it was decided to run a tensioned stainless steel shaft through the middle of the braided cable. The cable itself does not have the strength to survive the stresses and vibrations imposed on it by the test apparatus and the hydrodynamic forces.

Two cases will be considered in detail: A fixed-end attachment case where the test section is rigidly attached to the vertical strut, and a simply supported case where the test section is free to rotate on the vertical strut.



CATENARY EFFECTS LESS THAN 2%

Figure 2.1. Test Section Orientation

2.2 FIXED-END CONDITION

The test section can be considered as a beam fixed at both ends under axial tension. In addition there is a transverse load of drag forces, W , as shown in figure 2.2. The axial tension tends to straighten the beam and reduce the bending moment produced by the transverse loading. It will be assumed that the test section is 90 degrees to the flow, the most severe of any orientation.

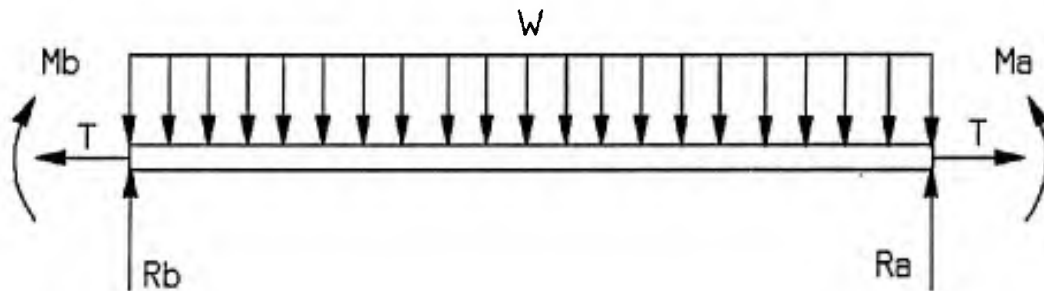


Figure 2.2 Fixed-End Condition

The governing equation for this system can be written as a second order differential equation in the form

$$EI \frac{\partial^2 Y}{\partial X^2} = M \quad (2.1)$$

where

$$M = V_0 X - \frac{1}{2} W X^2 + T Y - M_0. \quad (2.2)$$

Substituting the moment back into the first equation and rearranging, one finds that

$$EI \frac{\partial^2 Y}{\partial X^2} - T Y = -M_0 + V_0 X - \frac{1}{2} W X^2. \quad (2.3)$$

This differential equation is solved in conjunction with the force equations so that the deflections and stresses in the beam can be found. The solution of this differential equation is the sum of the homogeneous and particular solutions (reference 9). The homogeneous solution is found by assuming the solution to be of the form

$$Y(x) = e^{\lambda x}. \quad (2.4)$$

Substituting this back into the left side of the equation and setting equal to zero gives the following solution:

$$Y_H = C_1 e^{\sqrt{\frac{T}{EI}} x} + C_2 e^{-\sqrt{\frac{T}{EI}} x} \quad (2.5)$$

where

$$\lambda = \pm \sqrt{\frac{T}{EI}}. \quad (2.6)$$

The particular solution is assumed to be of the form

$$Y_p = A + BX + CX^2 \quad (2.7)$$

and

$$\ddot{Y}_p = 2C. \quad (2.8)$$

Putting this back into equation (1.1), one can show that

$$EI(2C) - T(A+BX+CX^2) = -M_o + V_o X - \frac{1}{2}WX^2. \quad (2.9)$$

Equating the two sides gives

$$A = \frac{M_o T + EIW}{T^2} \quad (2.10)$$

$$C = \frac{1}{2} \frac{W}{T} \quad B = -\frac{V_o}{T}.$$

Thus, the particular solution is shown to be

$$Y_p = \frac{M_o T + EIW}{T^2} - \frac{V_o}{T} X + \frac{1}{2} \frac{W}{T} X^2. \quad (2.11)$$

Adding the particular solution to the homogeneous solution gives the total solution:

$$Y = C_1 e^{\sqrt{\frac{T}{EI}} x} + C_2 e^{-\sqrt{\frac{T}{EI}} x} + \frac{M_o T + EIW}{T^2} - \frac{V_o}{T} X + \frac{1}{2} \frac{W}{T} X^2. \quad (2.12)$$

Using this equation, the sum of the forces in the y direction,

and the initial conditions, one can determine the constants C_1 and C_2 . The initial conditions are $X=0$ when $Y=0$ and $dY/dX = 0$ when $X = L/2$. With these conditions the two unknown constants can be found to be

$$C_2 = \frac{\frac{M_o}{T} + \frac{EIW}{T^2}}{1 - e^{-\sqrt{\frac{T}{EI}}L}} \quad (2.13)$$

and

$$C_1 = -\left[C_2 + \frac{M_o}{T} + \frac{EIW}{T^2}\right]. \quad (2.14)$$

Substituting C_1 and C_2 into equation 2.12 leaves it with two unknowns, Y and M_o . A third boundary condition can be used to satisfy this condition

$$\frac{\partial Y}{\partial X} = 0 \quad X = 0. \quad (2.15)$$

This gives an expression for M_o in terms of known quantities:

$$M_o = -\frac{T}{3} \left[\left(\frac{EIW}{T^2} + \frac{V_o}{T} \right) (1 + e^{-\sqrt{\frac{T}{EI}}L}) + 2 \frac{EIW}{T^2} \right]. \quad (2.16)$$

Equation (2.12) is coded so numerous options can be explored. Two aspects of the analysis will be considered: the mid-point deflection when $X = L/2$, and the stress at the end point. The end moment for numerous cases will be reviewed. Finally, the Von Mises failure criterion will be

used to compute the maximum stress in the test section (reference 10). This will take the form

$$\sigma_{\max} = \left[\left(\frac{T}{A} + \frac{M_o C}{I} \right)^2 + 3 \left(\frac{4}{3} \frac{V_o}{A} \right)^2 \right]^{\frac{1}{2}} \quad (2.17)$$

and will be computed at the end point.

The fixed geometric conditions are given as design constraints. The maximum diameter for the stiffening rod is determined by the internal diameter of the flexible hose. The maximum total length of the test section is determined by the dimensions of the Langley Tow Tank Facility (reference 11). The estimated distributed load caused by hydrodynamic drag is calculated from the outside diameter of the flexible hose (reference 12):

$$W = \frac{1}{2} \rho V^2 C_{dn} D. \quad (2.18)$$

Graphs that follow indicate various loading situations for the given design constraints. The focus of this initial study will be a flexible spiral wound cable that has an internal diameter of 0.4 inch, an outside diameter of 0.625 inch, and an estimated normal drag coefficient of 1.39 (reference 13). Two test section lengths will be considered: one that is 96 inches long and another that is 60 inches

long.

Figure 2.3 is the end-moment graphed with the in-line tension for various velocities. For each test case it can be seen that as the in-line tension is increased the end-moment is reduced. This reduces the Von Mises stress at the end point. The design goal, where mid-point deflection is less than 2 percent of the test section length, implies that the minimum in-line tension must be on the order of 2000 pounds. This means that the stiffening rod must be able to handle 130,000 to 140,000 psi without failing. Figure 2.4 represents mid-point deflection graphed against the in-line tension for numerous velocities. Figure 2.5 is the calculated stress at the end plotted against in-line tension for various velocities.

END MOMENT VS TENSION

FIXED END CONDITION

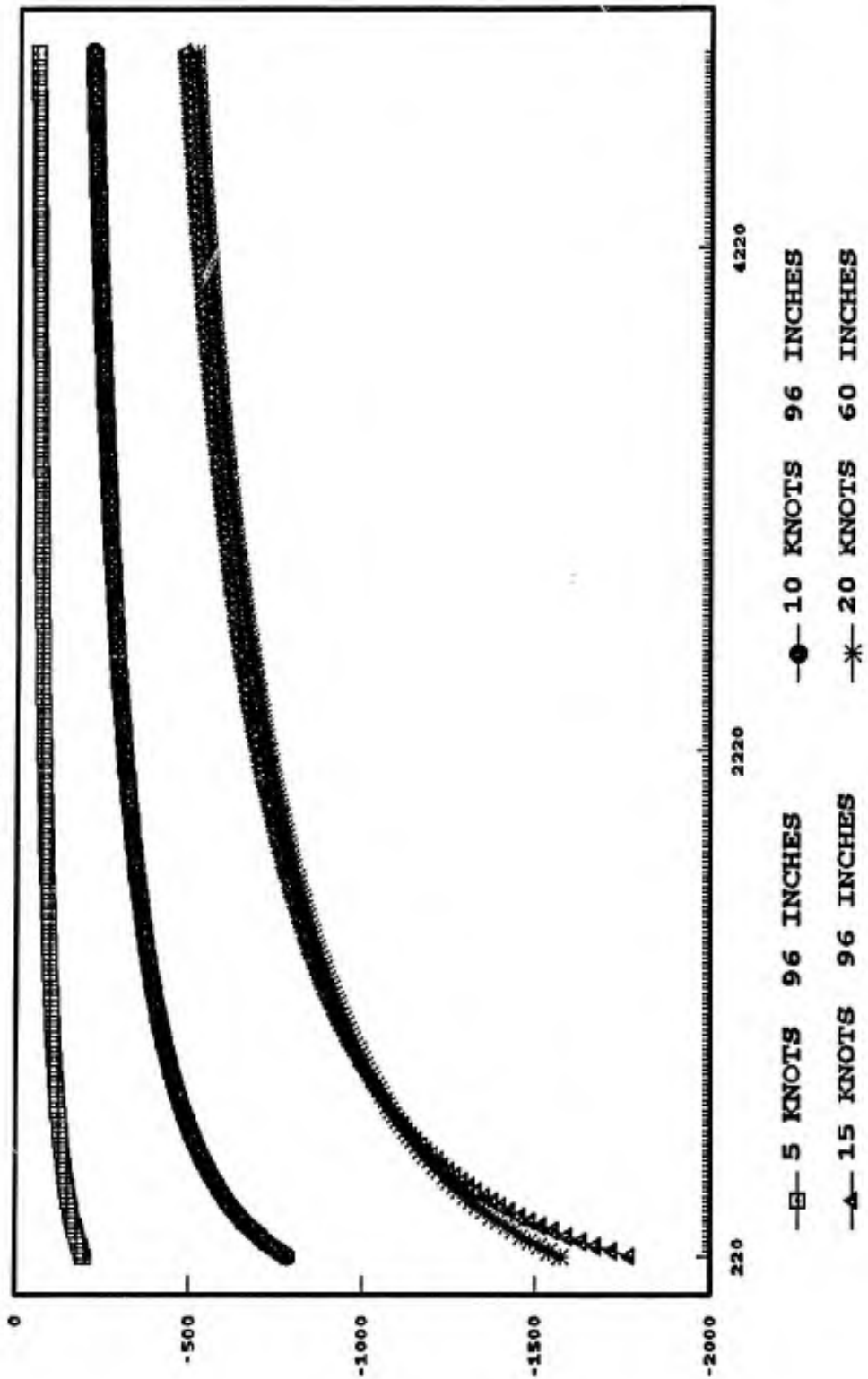


Figure 2.3. End Moment vs Tension at Fixed End

DEFLECTION VS TENSION

FIXED END CONDITION

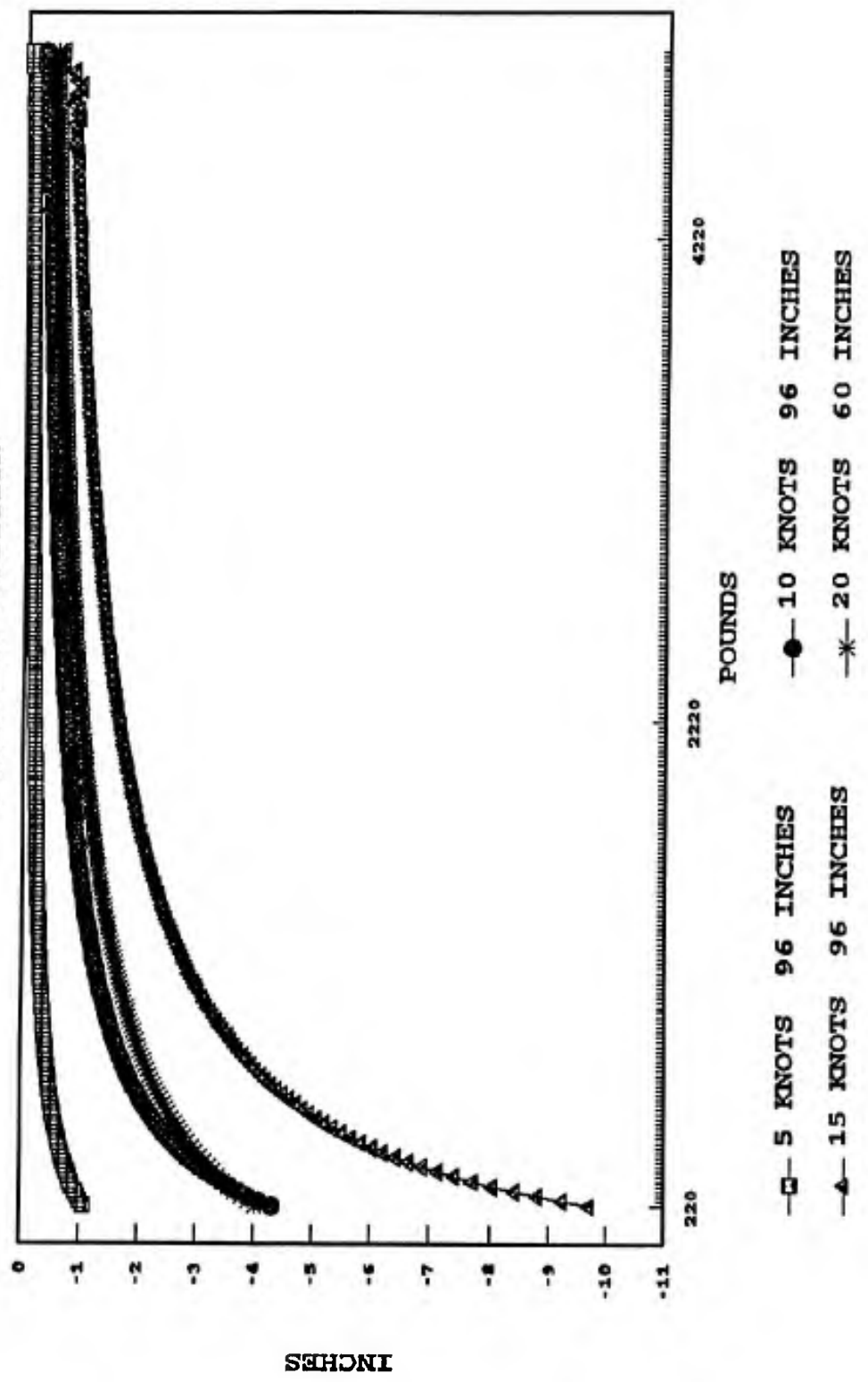


Figure 2.4. Mid-Point Deflection vs Tension at Fixed End

VON MISES STRESS VS TENSION

FIXED END CONDITION

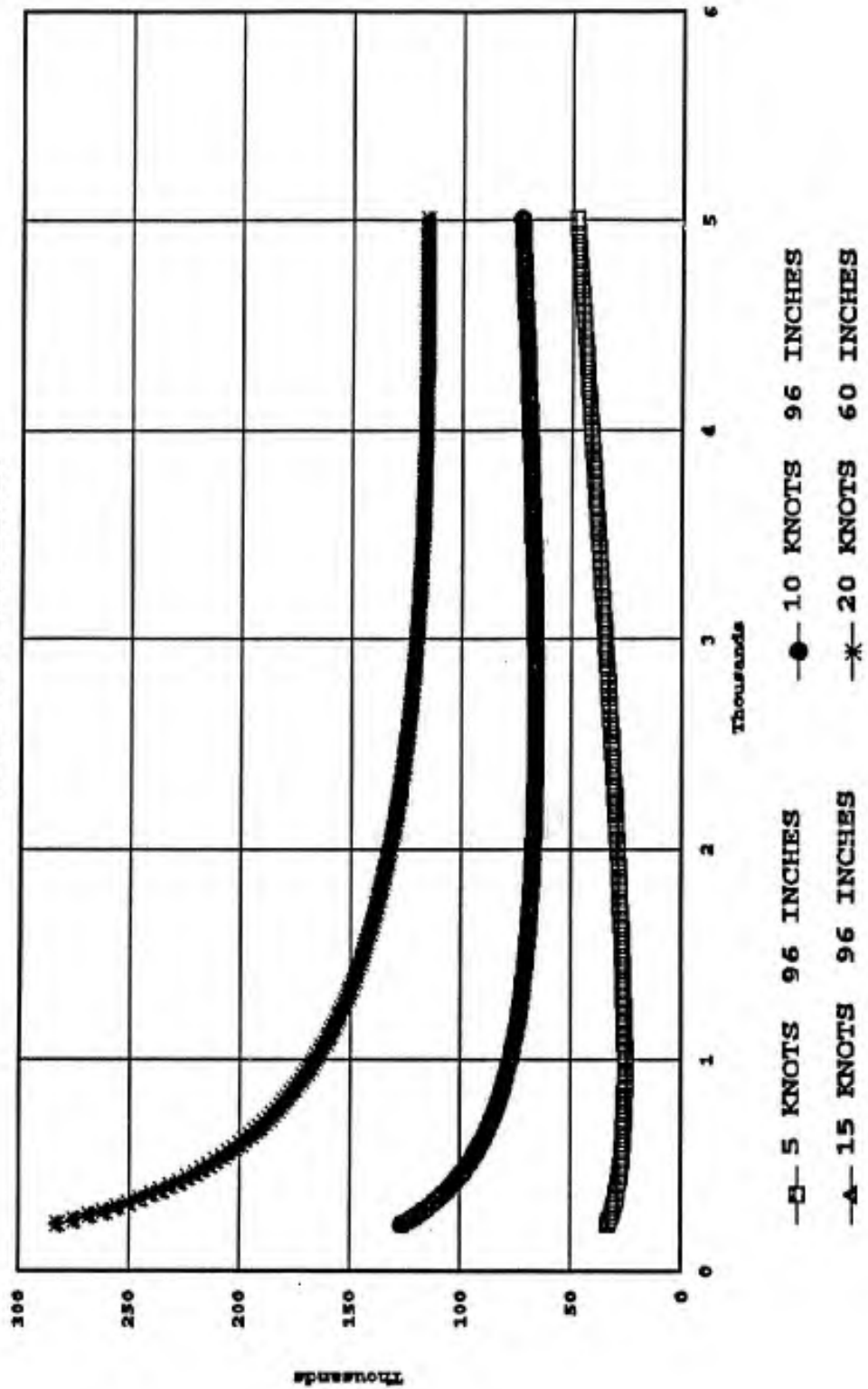


Figure 2.5. Von Mises Stress vs Tension at Fixed End

2.3 SIMPLY SUPPORTED CONDITION

This case considers that the test section is a beam supported at both ends but free to rotate, figure 2.6. The stiffener is under axial tension and a uniform cross load caused by the fluid drag.

The governing equation for this system can be written as a second-order differential equation of the form

$$E I \frac{\partial^2 Y}{\partial X^2} = M. \quad (2.19)$$

In this case there is no moment at each end of the test section.

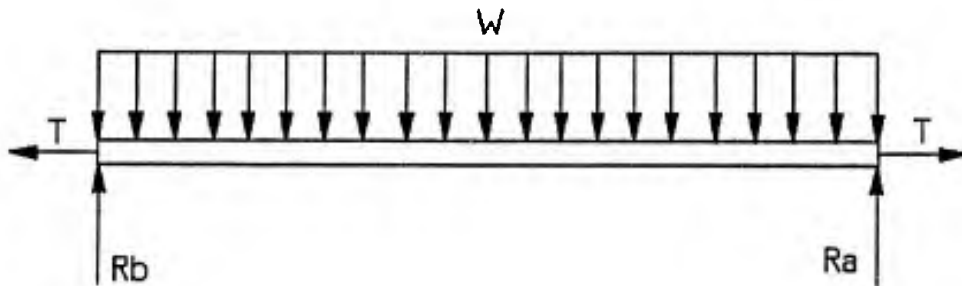


Figure 2.6 Simply Supported Condition

The governing equation is

$$EI \frac{\partial^2 Y}{\partial X^2} = V_0 X - \frac{1}{2} W X^2 + T Y. \quad (2.20)$$

The homogeneous solution remains the same as in the fixed-end condition, so that

$$Y_H = C_1 e^{\sqrt{\frac{T}{EI}} X} + C_2 e^{-\sqrt{\frac{T}{EI}} X}. \quad (2.21)$$

The particular solution is also in the same form as the fixed end solution. Putting this into equation (2.20) gives

$$EI(2C) - T(A + BX + CX^2) = V_0 X - \frac{1}{2} W X^2. \quad (2.22)$$

By equating the two sides it can be shown that

$$A = \frac{EIW}{T^2} \quad B = -\frac{V_0}{T} \quad C = \frac{1}{2} \frac{W}{T}. \quad (2.23)$$

So the particular solution is shown to be

$$Y_p = \frac{EIW}{T^2} - \frac{V_0}{T} X + \frac{1}{2} \frac{W}{T} X^2. \quad (2.24)$$

Adding the particular solution to the homogeneous solution gives

$$Y = C_1 e^{\sqrt{\frac{T}{EI}} X} + C_2 e^{-\sqrt{\frac{T}{EI}} X} + \frac{EIW}{T^2} - \frac{V_0 X}{T} + \frac{1}{2} \frac{W}{T} X^2. \quad (2.25)$$

The constants C_1 and C_2 are found using the initial conditions $X = 0$ when $Y = 0$, and $dY/dX = 0$ when $X = L/2$; thus,

$$C_1 = -\frac{\frac{WEI}{T^2}}{1 - e^{-\sqrt{\frac{T}{EI}}L}} - \frac{WEI}{T^2} \quad (2.26)$$

$$C_2 = \frac{\frac{WEI}{T^2}}{1 - e^{-\sqrt{\frac{T}{EI}}L}} \quad (2.27)$$

Equation (2.25) is coded so that numerous options can be explored. Two aspects of the analysis are integral to the test section design: the mid-point deflection and the stress at the end point.

Since this is a simply supported condition there is no end moment. Figure 2.7 is the Von Mises stress plotted against the in-line tension for numerous velocities. Figure 2.8 is the mid-point deflection plotted against the in-line tension for numerous velocities. In order to obtain the desired mid-point deflection, an in-line tension on the order of 2000 pounds is again required. This yields a considerably smaller maximum stress at the end point, which is on the order of 15,000 to 25,000 psi.

VON MISES VS TENSION

SIMPLY SUPPORTED

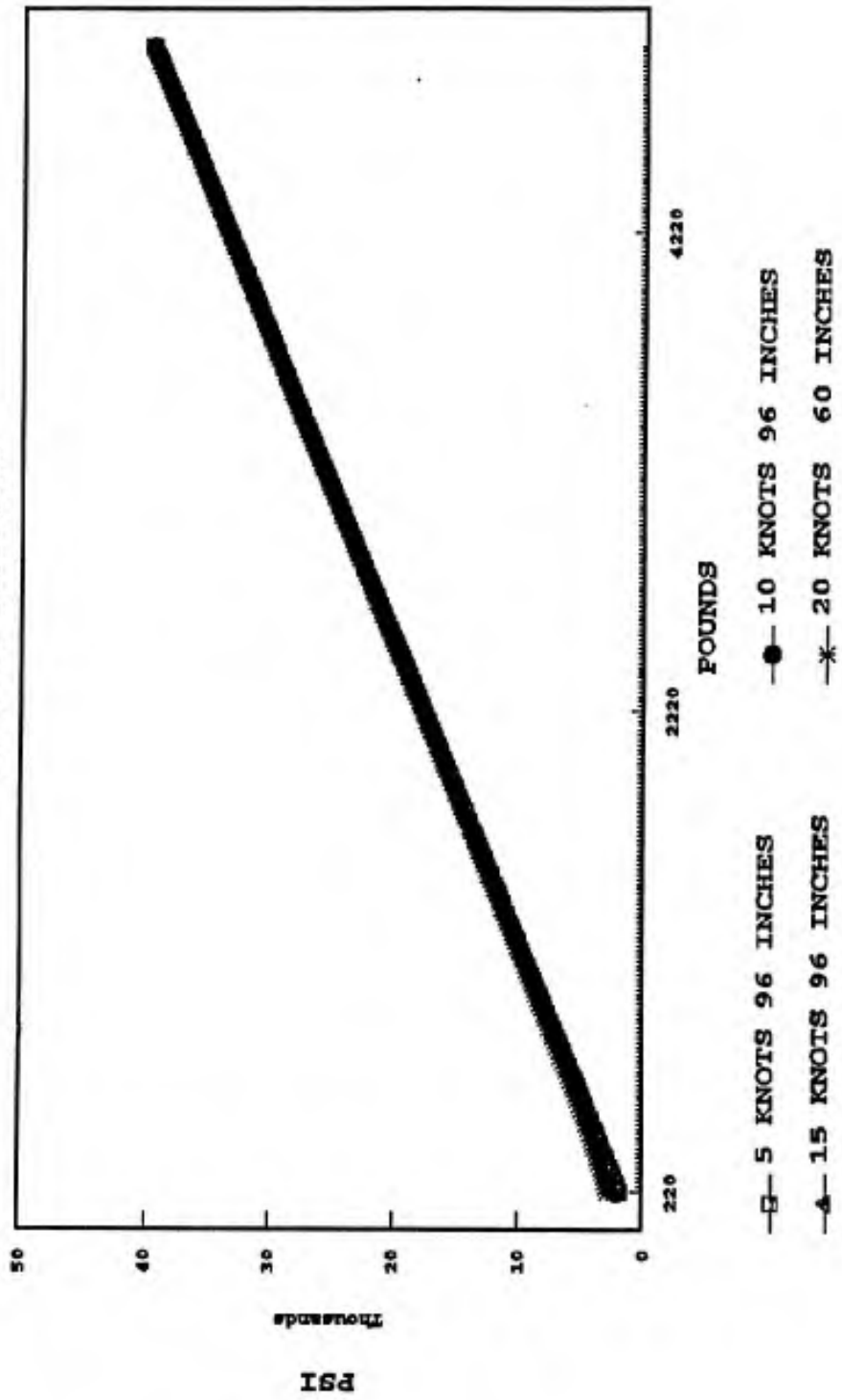


Figure 2.7. Von Mises Stress vs Tension, Simply Supported

DEFLECTION VS TENSION

SIMPLY SUPPORTED

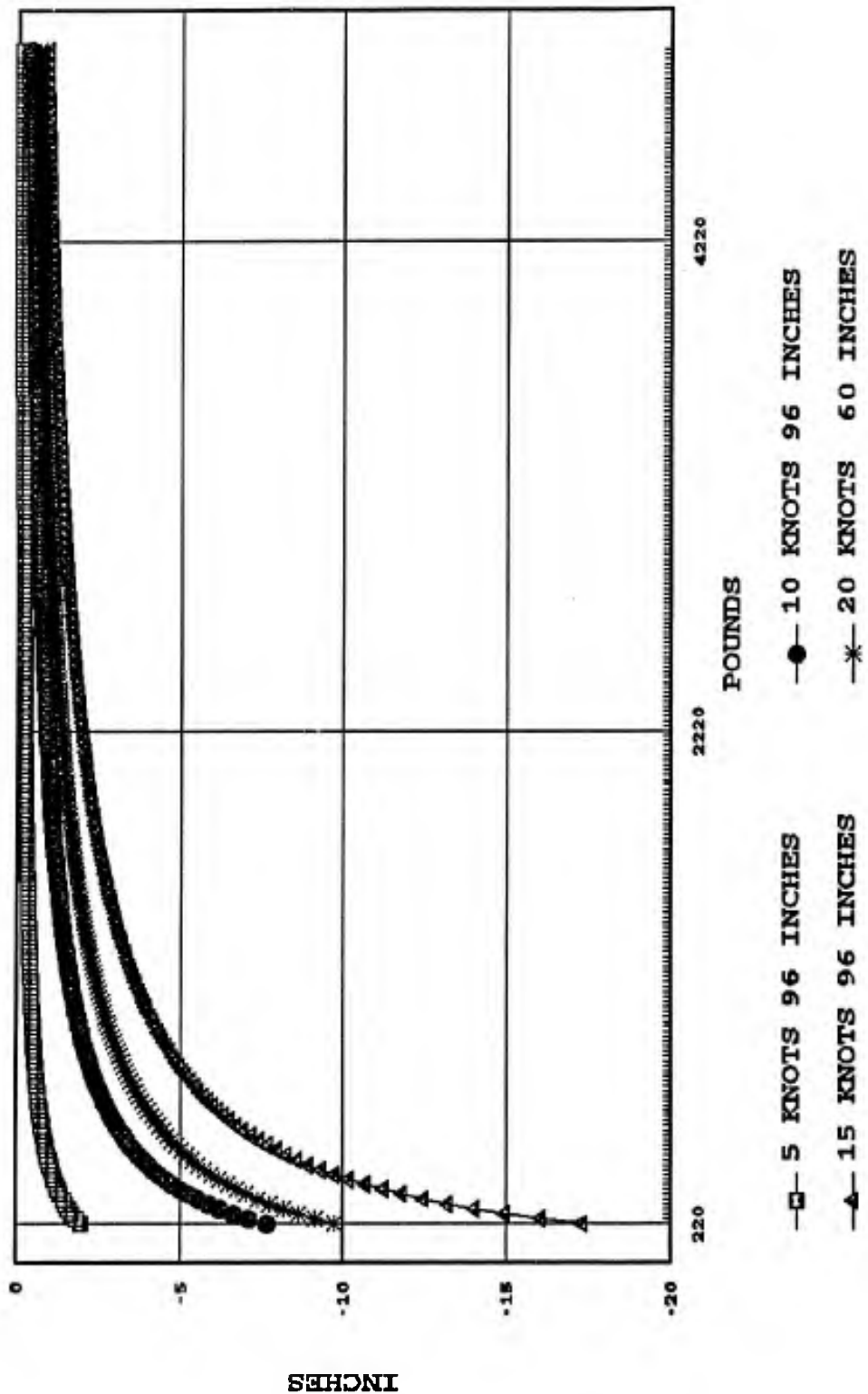


Figure 2.8. Mid-Point Deflection vs Tension, Simply Supported

2.4 TEST SECTION DESIGN

It should be remembered that the hydrodynamic loading of the test section was estimated. This was necessary to compute the test section reactions but might lead to false confidence in the absolute numbers of stress and deflection at various velocities. Further, it should be noted that vortex shedding on the test section is a real phenomenon that has been neglected. Vortex shedding might cause oscillations of the test section, which in turn would increase the effective frontal area, which then increases the hydrodynamic load. Finite element models have been constructed to address these issues and are presented in chapter 4. These models are able to predict the modal response of the drag apparatus, which will aid in determining if resonant vibrations occur.

It is evident after reviewing the fixed-end and simply supported end conditions of the test section that both are capable of reducing the catenary to 2 percent of the overall length. The fixed-end condition has significantly higher stress at the end points. While this is a disadvantage when considering stress, it might prove beneficial when considering the mounting of strain transducers.

With these end conditions evaluated it is now possible to consider in detail the methodology to be used to instrument the ends of the test section to measure the hydrodynamic load directly.

CHAPTER 3: INSTRUMENTATION

3.1 TRANSDUCER SETUP

To accurately determine the hydrodynamic loads acting on the test section it is necessary to measure the in-line forces at the end of the test section. In both the simply supported and the fixed-end conditions, strain transducers will be used to accomplish this task. It is felt that strain transducers are best suited for this particular application (reference 14). These transducers will provide the best accuracy while avoiding the cost of a more expensive system.

In the preceding chapter, significant effort was made to determine the reaction forces and stresses at the end of the test section. It was determined that the stress in both cases was greatest at the ends of the test section. This fact, coupled with ease of orientation, dictates the location of the transducers. Load cells that can accurately measure high in-line forces, as well as smaller off-axis forces, are not available; thus, a force transducer was designed for this application.

The mechanical design of these transducers will be addressed separately for the simply supported condition and the fixed-end condition. For environmental reasons, stress requirements, and strain sensitivity, the material selected for both transducers is stainless steel 17-4ph (reference 15).

Important design criteria for each case will be based on linear and uniform strain contours. It is considered that if the material where the strain rosettes are mounted has a strain field that is uniform, the results of the experiment will be more accurate.

Significant effort has been devoted to determining the end loads so that a stiffening rod may be used with the apparatus design to reduce potential catenary problems. This analysis assumes uniform drag loading of the test section. The predicted end loads are used to design the strain transducers.

3.2 SIMPLY SUPPORTED CASE

From chapter 2 one can see that the maximum end load occurs for the simply supported case when the apparatus is moving at 15 knots. In this condition, the end forces are 2220 pounds in tension and 180 pounds in shear with zero moment. There are three options available to measure the shear and tension forces: (1) Measure them directly with a biaxial strain transducer. Given the nature of the stress in this condition, this method would ~~not~~ give sensitive shear values. (2) Measure the in-line tension and the angle of rotation at the end point. Since the angle of rotation is so small this would be very difficult. (3) Measure the resultant force and calculate the angle of rotation. To calculate the

angle of rotation the governing equation in chapter 2 could be used for the case that is 90 degrees to the flow. For other orientations a differential equation that considers a more general equation must be derived.

It is assumed that the body of the transducer is a beam simply supported on one end with a load applied on the other end (see figure 3.1). With a predicted maximum load of 2220 pounds and a desired stress state of 130,000 psi, the desired cross sectional area can be calculated in a rather trivial manner. If the outside diameter, is chosen to be close to the test section diameter, then the internal diameter can be chosen directly:

$$\sigma = \frac{T}{A} \quad \text{where} \quad A = \pi R^2 - \pi r^2. \quad (3.1)$$

Since the beam is in pure tension, the strain field will be completely uniform.

The simply supported condition proves to be more complicated than the fixed-end condition because the measured quantities are used in conjunction with the governing equations to obtain a solution. Errors are propagated through the governing equations, which increases the uncertainty of the solution. To quantify the significance of this problem an uncertainty analysis should be completed.

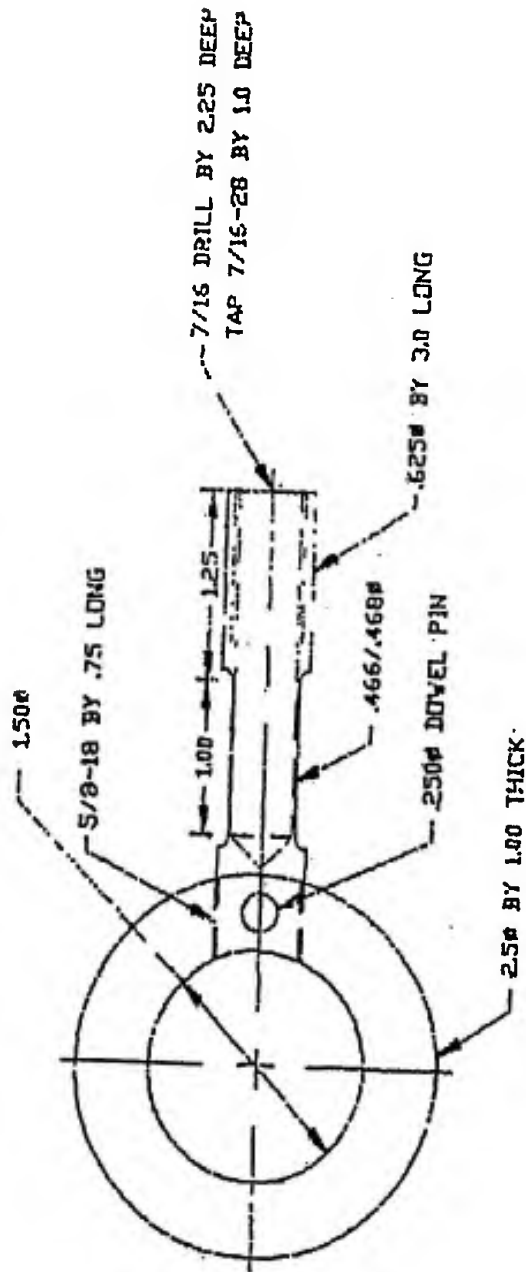


Figure 3.1. Simply Supported Transducer

3.2 FIXED-END CONDITION

In the fixed-end condition the inverse solution technique is used to design the transducer. It is assumed in this case that the body of the transducer is a beam fixed on one end with a load applied on the other end (see figure 3.2). The transducer cross section is optimized so that it holds the maximum expected load of 2000 pounds in pure tension, 180 pounds of shear, and 707 inch-pounds of moment, while giving the sensitivity to accurately measure the shear and tension forces.

By making a rectangular cross section one increases the sensitivity of the shear measurement while holding the tension stress constant. Holding large in-line tensions while remaining sensitive to the shear loading is an ideal situation for a biaxial strain transducer. If this can be done and only small strain gradients are created, a solution has been found. The design variables are the height, length, and width of the rectangular cross section.

From the Von Mises stress equation,

$$\sigma = \left[\left(\frac{P}{A} - \frac{Mc}{I} \right)^2 + 3\tau^2 \right]^{\frac{1}{2}} \quad (3.2)$$

$$\tau = \frac{4}{3} \frac{R}{A} \quad I = \frac{db^3}{12} \quad A = bd.$$

With the dimensions shown in figure 3.2, it is calculated that the bending moment is 91.3 percent of the total stress contribution. This insures sufficient strain length to obtain

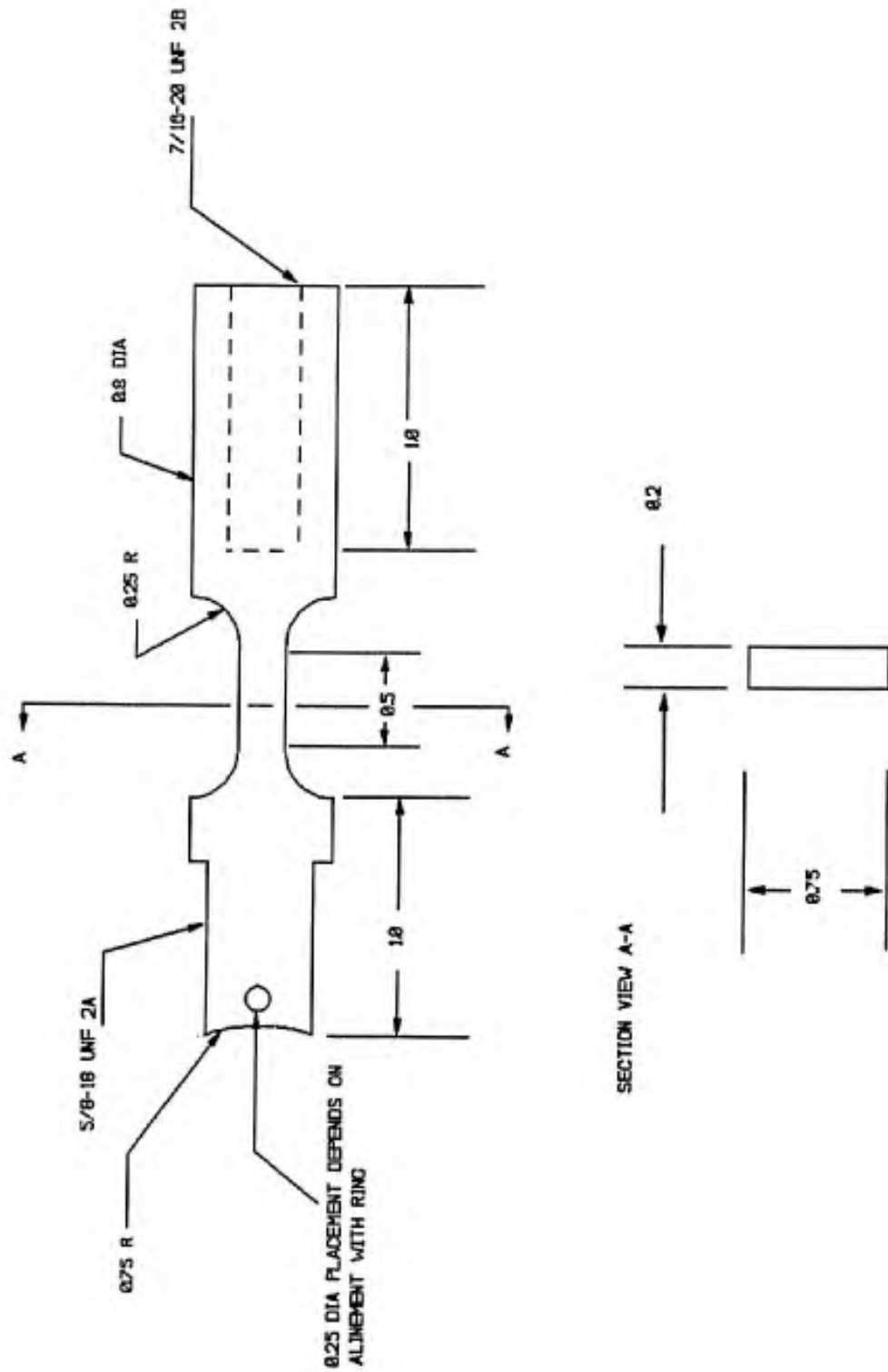


Figure 3.2. Fixed-End Transducer

shear force accuracy.

A three-dimensional mathematical model of the fixed beam was created in ABAQUS finite element code to aid in the design of the strain transducer (reference 16). This model was used to calculate stress values in the cross section; these values were similar to those obtained by direct calculation. The model also showed predicted strain contours that indicated that there were no adverse strain gradients.

A mesh of the model is shown in figure 3.3. The model is built from eight-node, linear displacement bricks. The basic geometry was created in a solid model package. A mesh generator was used to create the full mesh. All the nodes on the right face were grouped together into a node set so that the predicted loads could be applied. All the nodes on the left face were fixed in space. A linear step analysis was selected that indicated that the stiffness matrix should be formed at the first increment and then used throughout the entire step. This step was analyzed as a static load step with the basic tolerances for the solution of the equilibrium equations being set to 0.1 pound of all the forces at each node.

The results of the stress analysis are shown graphically in figures 3.4 through 3.9. It can be seen that the maximum predicted stress is within 5 percent of the calculated value. Also, it is evident that in the middle of the transducer there are no adverse strain gradients.

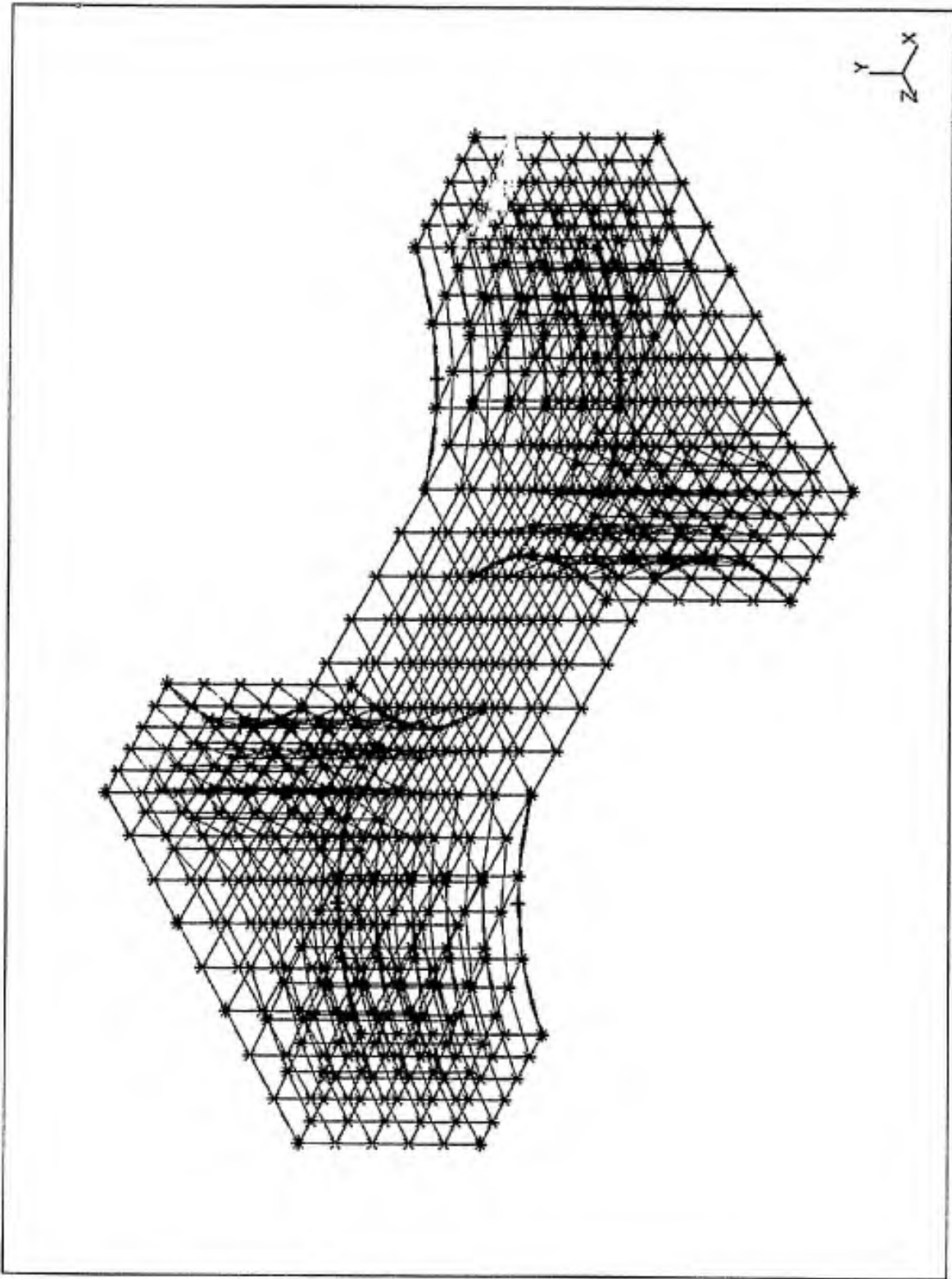


Figure 3.3. Mesh of Transducer

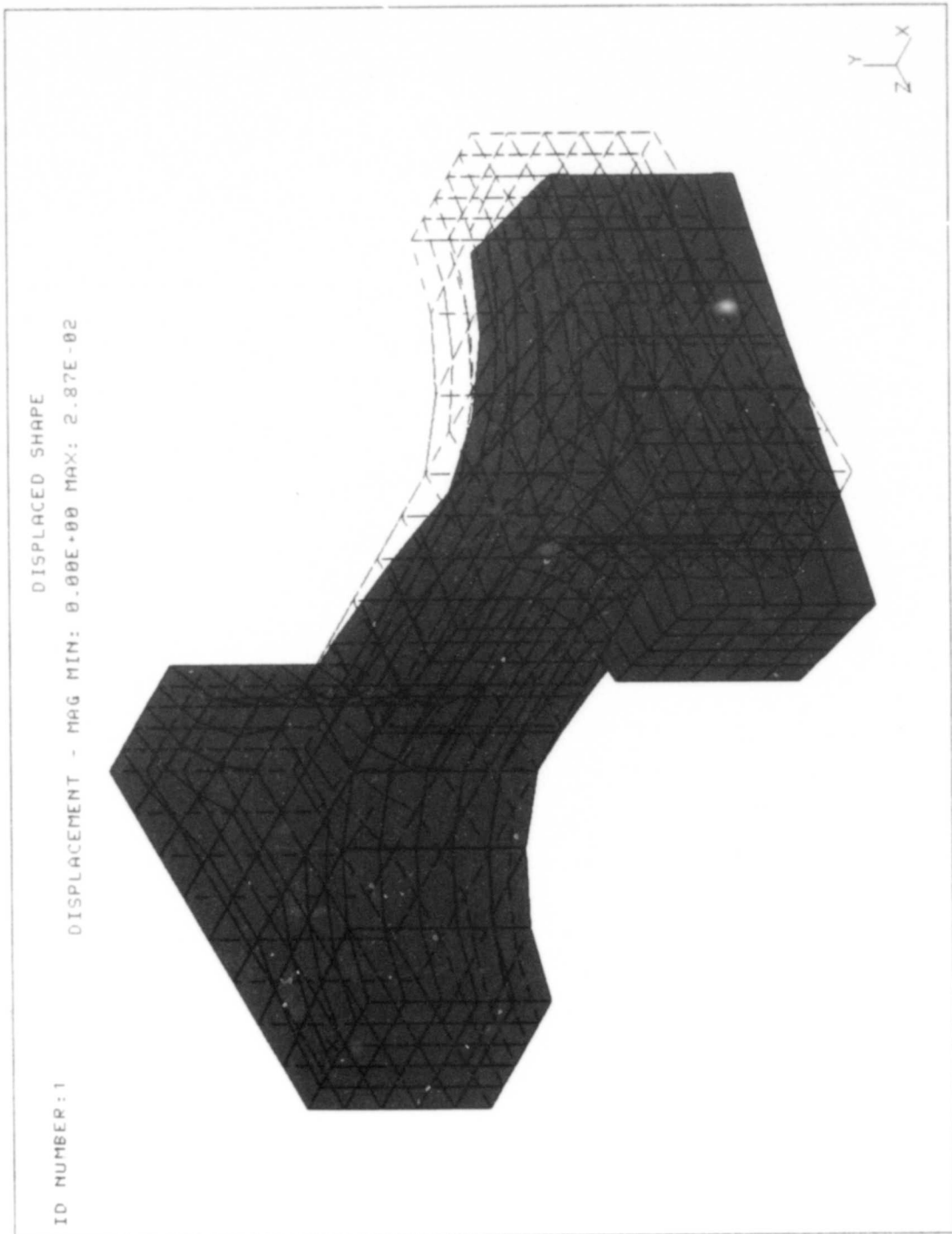


Figure 3.4. Deflection of Transducer

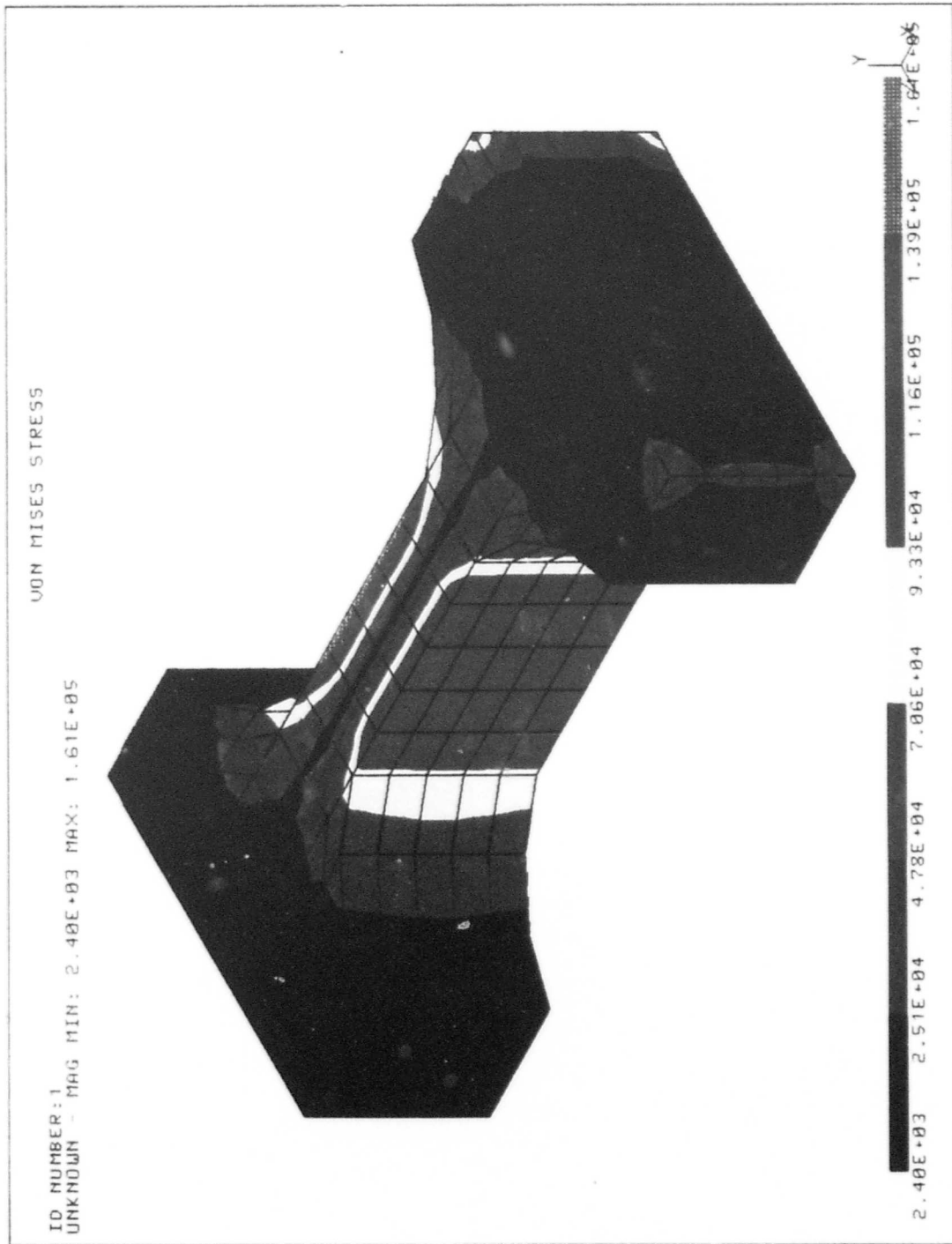


Figure 3.5. Von Mises Stress, Bird's Eye View

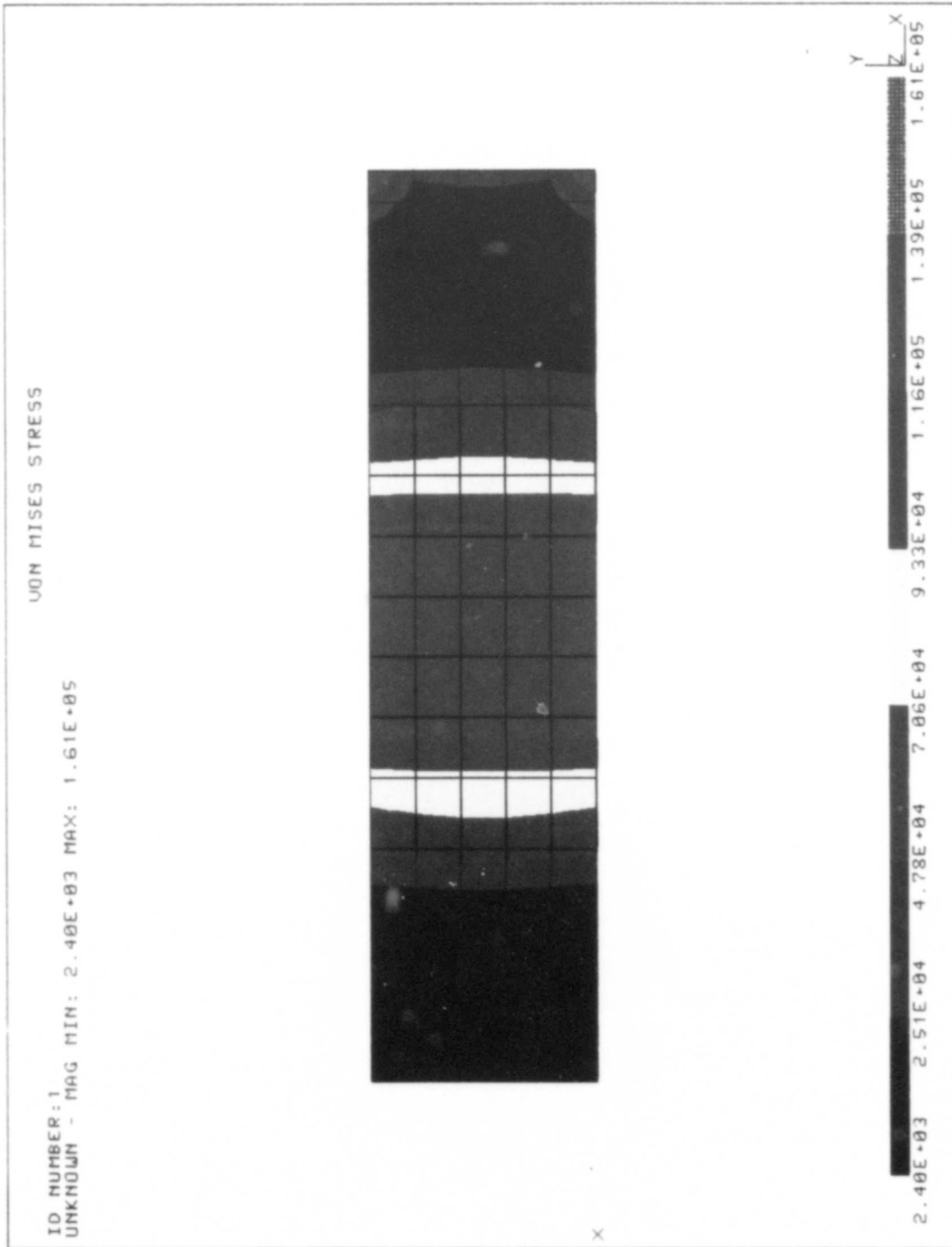


Figure 3.6. Von Mises Stress, Back View

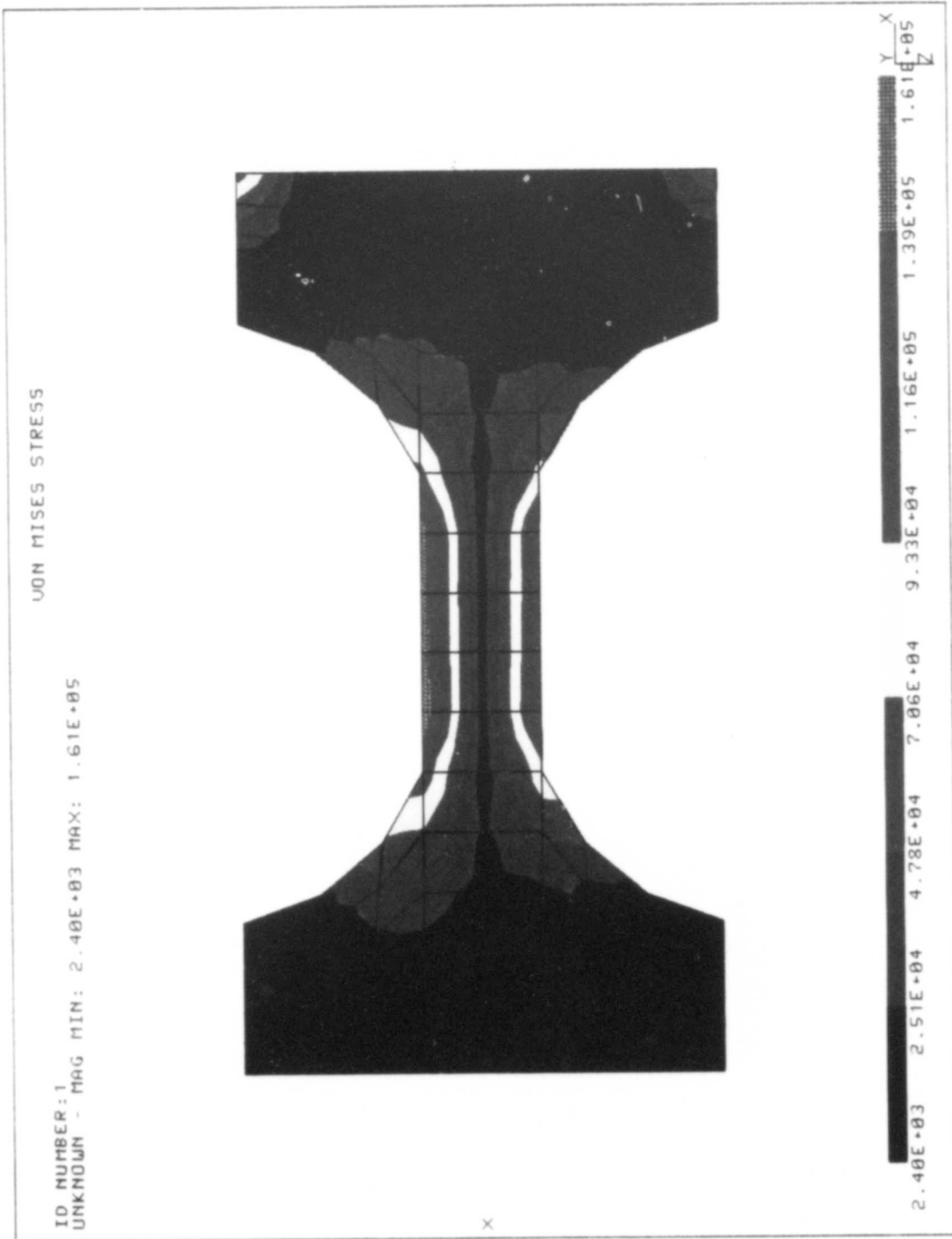


Figure 3.7. Von Mises Stress, Top View

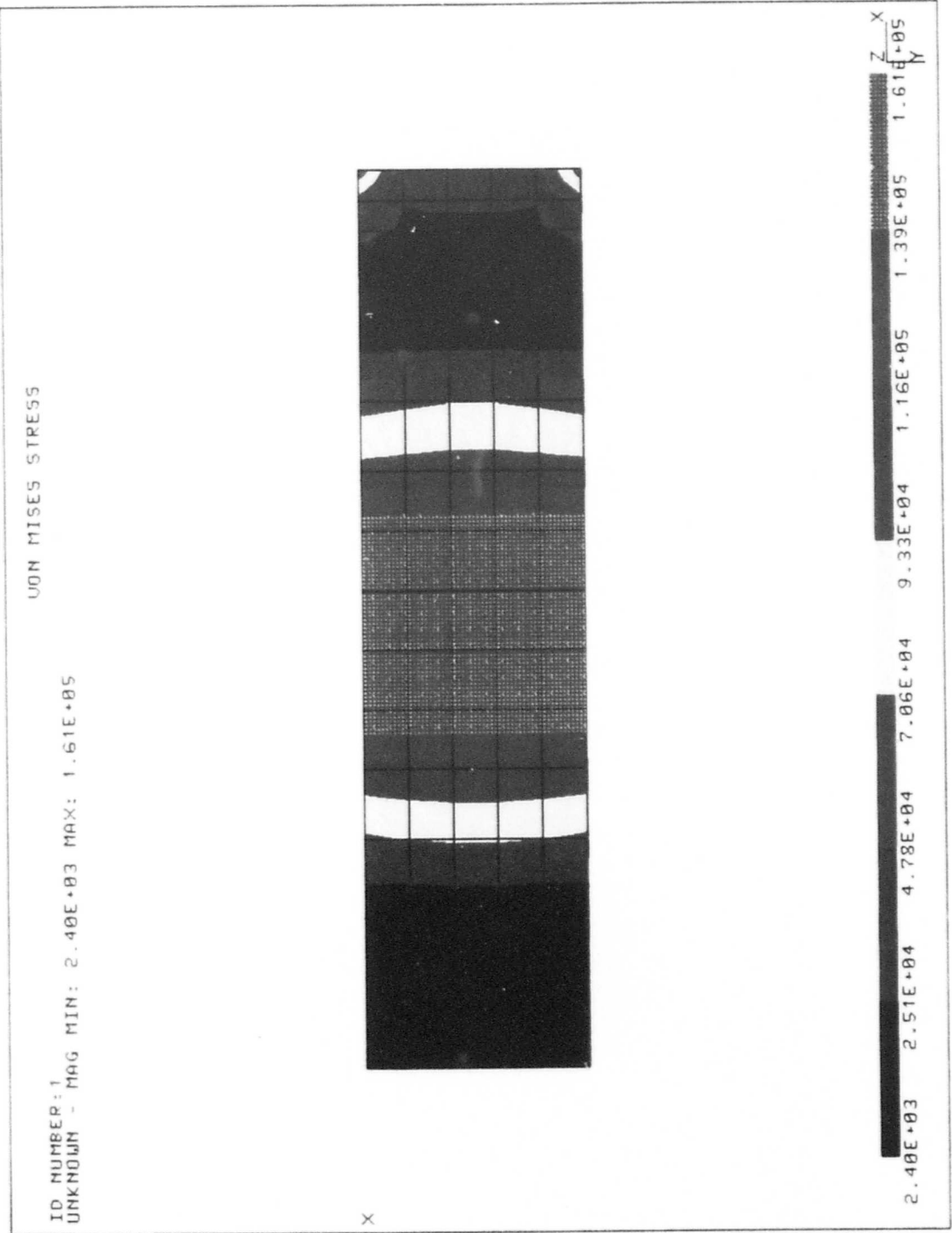


Figure 3.8. Von Mises Stress, Front View

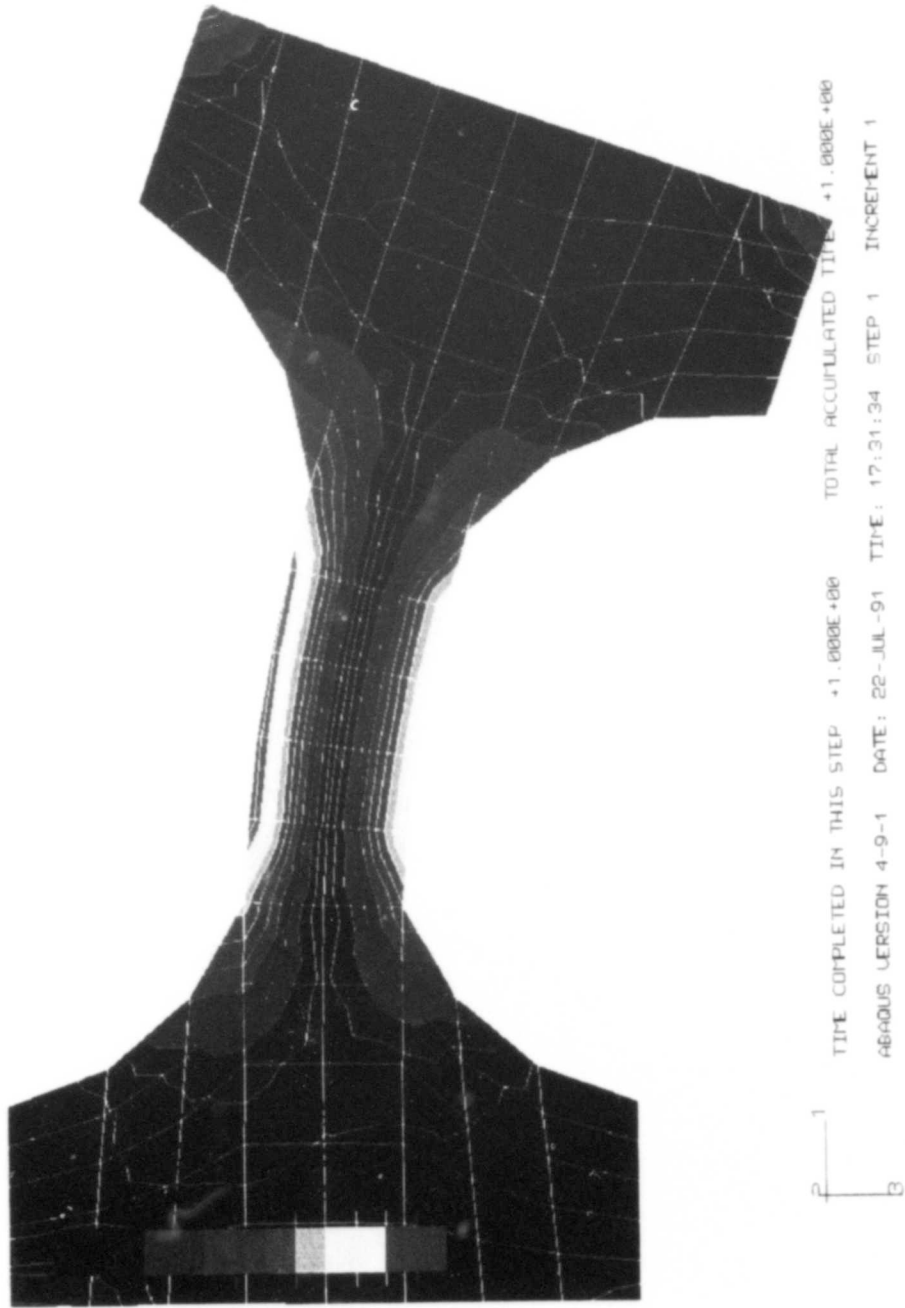


Figure 3.9. Von Mises Stress, Deflected

3.4 COMPARISON OF THE END CONDITIONS

It can be seen that the simply supported case has the inherent problem of being dependent on theoretical calculations when computing the normal hydrodynamic drag coefficient. Errors in the measured values will propagate through the governing equations and increase the uncertainty of the solution. There is merit to using this type of setup when measuring the tangential drag coefficient because the tangential force is measured directly, making the calculation of the tangential coefficient straight-forward.

By designing the cross sectional area of the fixed-end transducer in the form of a rectangle and making its height-to-width ratio almost 4 to 1, one can obtain accurate measurements. This design allows for the bending moment to contribute 91.4 percent of the total stress, which makes it highly sensitive to the shear load and thus a good place to mount a bi-directional strain rosette.

CHAPTER 4: VIBRATION ANALYSIS

4.1 INTRODUCTION

In an effort to determine the adequacy of the drag apparatus when considering vibration isolation of the test section, the natural frequencies of vibration have been computed using the ABAQUS finite element code (reference 16). The fundamental frequency of the test section is compared to the extracted value computed by ABAQUS. The anticipated vortex shedding frequencies are calculated at different locations in an effort to determine if resonant excitations are present. Displacement data and stress information are compared to the chapter 2 calculations. The focus of this chapter is two-fold: first, to determine if the drag apparatus isolates vibrations from the strain transducers and the test section; and, second, to cross-check calculations presented in chapter 2.

4.2 EIGENVALUE EXTRACTION

The finite element model (FEM) of the drag apparatus, figure 1.7, is created with 210 two node beams as shown in figure 4.1. Distributed loads representing the hydrodynamic drag are placed on the test section and supports. A point load is placed on node 147 to simulate the tensioning system. Only half of the apparatus is modeled since it is symmetric. The test section is 96 inch long and 0.625 inch in diameter.

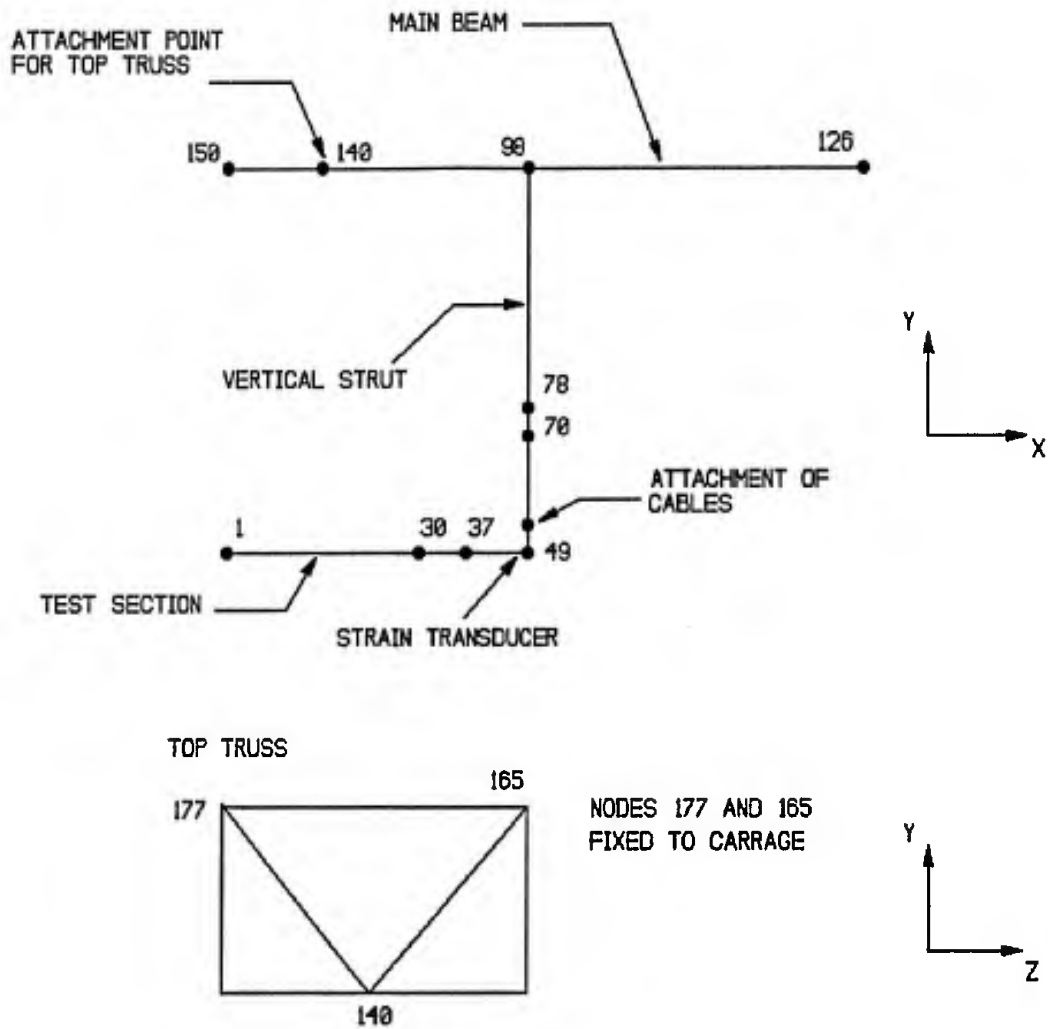


Figure 4.1. Beam Model of Drag Apparatus

The vertical struts are 48 inches long and 2.5 inches in diameter. The supporting I-beam is 16 feet long and is a standard W6-25 flange. The truss that connects the I-beam to the tow carriage is made from 3 by 3 by 3/8-inch box beams. The support cables are 12 feet long and 0.5 inch in diameter. Beam elements that represent this basic structure are created in ABAQUS and the natural frequencies are extracted. The extracted frequencies in this analysis are only numerical solutions and do not predict the magnitude of vibration. A forced response analysis would be the next step for this vibration analysis.

It should be noted that the added mass of the water is not considered in this analysis. The added mass effect of the water would have the effect of reducing the frequency response of the submerged sections of the apparatus. If the natural modes of vibration are close to the forced vibration, this added mass cannot be neglected.

Natural frequencies and the normalized displacements are extracted from the FEM model. This enables a comparison of the normalized displacements in the structure. Then, predictions on how vibrations are transferred to and from different sections can be made. The structure can be broken down into three distinct components: the main beam, the test section, and the vertical struts. Each component has its own fundamental modes of vibration. The "high frequency" modes will be neglected because the maximum normalized displacements

are significantly smaller than displacements at the low modes. This is based on the assumption that the energy of a given mode will be reduced as the modes reach high frequencies. Thus, it is necessary to consider only the lower order frequencies because they will be the worst case.

The I-beam has one fundamental mode of vibration at 1.1 Hz in the flow direction. In this case, the strain transducer's normalized displacement is 2.9 percent of the maximum normalized displacement. The I-beam has another fundamental mode predicted at 3.5 Hz in the y direction. The strain transducer's normalized displacement in this case is less than 1.0 percent of the maximum normalized displacement. In either case there is no appreciable transfer of vibration in the structure.

The test section has its predicted fundamental mode of vibration at 1.4 Hz, see figure 4.2. The strain transducer's normalized displacement is about 4.0 percent of the maximum normalized displacement. There is no appreciable transfer of vibration in the structure.

The vertical strut has its predicted fundamental frequency at 5.4 Hz, figure 4.3, and again at 8.4 Hz, figure 4.4. The strain transducer's normalized displacements are 27.2 percent and 36.2 percent of the maximum displacement respectively. There is a transfer of vibration from the strut to the test section, to the main beam, and to the support cables.

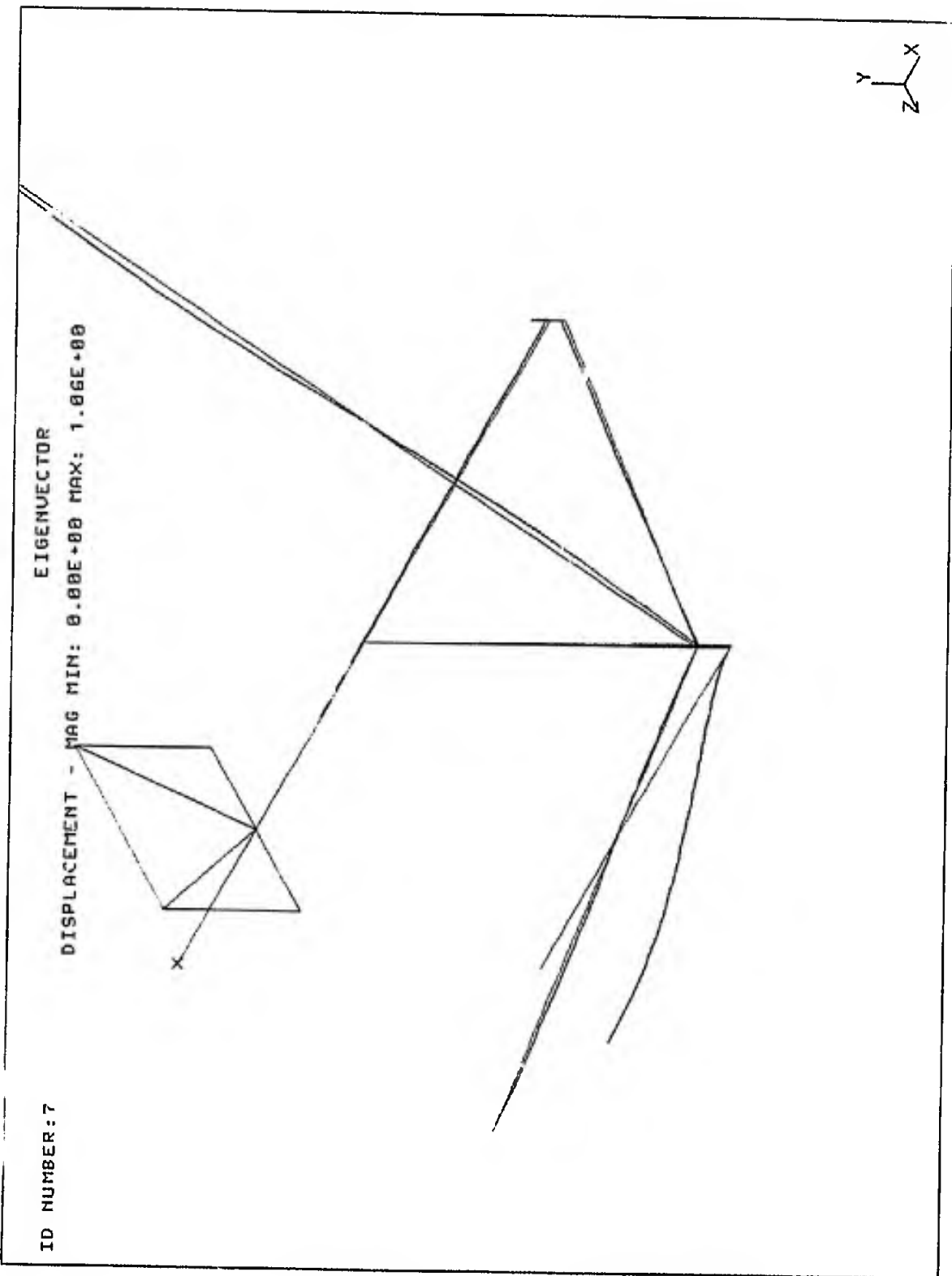


Figure 4.2. Test Section Fundamental Mode

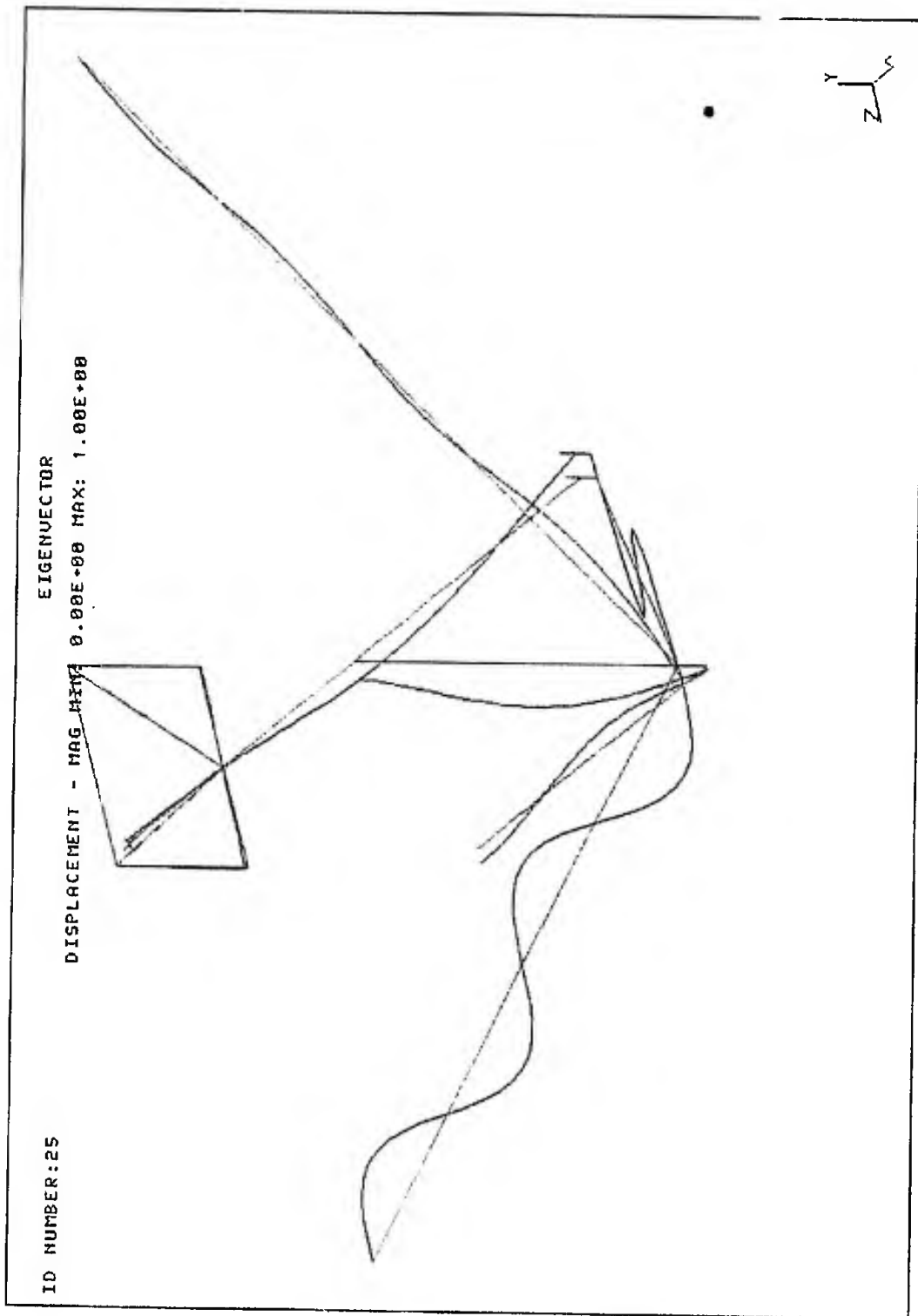


Figure 4.3. Vertical Strut Fundamental Mode

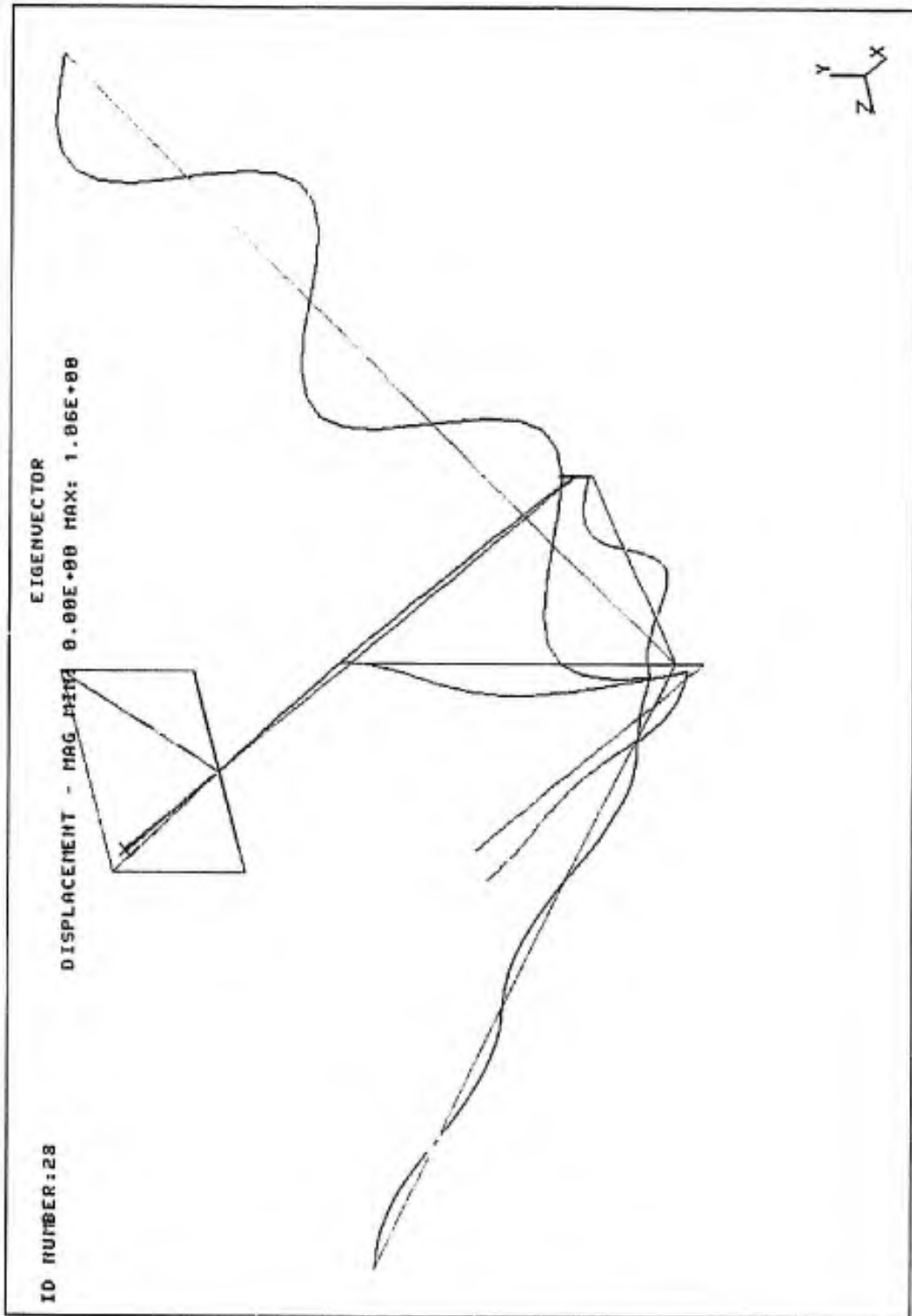


Figure 4.4. Vertical Strut Second Fundamental

These fundamental modes are considered the worst case scenario, but it should be noted that the first 50 eigenmodes, which include at least the third harmonic of the principal sections of the structure, all vibrate at a frequency of less than 10 Hz. This value will become important when the possible excitation sources are evaluated. If there is an excitation source close to any of the fundamental frequencies, resonant vibrations could occur.

4.3 VORTEX SHEDDING

When a long, unstreamlined body (such as a circular cylinder) is placed in a flow field, it can undergo flow excited transverse oscillations. These oscillations are the result of the periodic shedding of vortices from the upper and lower surfaces of the object. If the body is rigidly supported the vortices are shed at the Strouhal frequency (reference 17). This vortex shedding will be the primary excitation present in the drag apparatus, so the shedding frequency is calculated for the test section and the vertical struts. It is felt that if these shedding frequencies are different enough from the natural frequencies of the drag apparatus, resonant oscillations will not occur.

The Strouhal number for circular cylinders has been measured to be 0.21 for Reynolds numbers of 1500 to 150,000 (reference 18). The Strouhal number is a dimensionless

coefficient of the form

$$St = \frac{\omega D}{2 \pi U} \quad (4-1)$$

The following table lists the various speeds and potential excitation frequencies.

SPEED IN KNOTS	TEST SECTION	VERTICAL STRUT
5	32.4 Hz	8.1 Hz
10	64.8 Hz	16.2 Hz
15	97.2 Hz	24.3 Hz
20	129.6 Hz	32.4 Hz

It is readily seen that the excitation frequencies will be far above the fundamental resonant frequencies of every major section of the drag apparatus. Further, fairings will be placed on the vertical strut and all attached cables. These fairings will reduce drag forces and eliminate vortex shedding.

4.4 COMPARISON OF FEM AND CALCULATED VALUES

The fundamental frequency of the test section can be calculated analytically (reference 17). The solution of the governing differential equation reduces to

$$\omega_n = \sqrt{\left(\frac{N\pi}{L}\right)^2 \frac{T}{M} + \left(\frac{N\pi}{L}\right)^4 \frac{EI}{M}} \quad (4-2)$$

where $N=1$, $L=96$ " , $T=2323$ lb, $M=0.0359$ lb/in. , $I=1.256 \times 10^{-3}$ in⁴. , and $E= 30,000,000$ psi. The fundamental natural frequency is 1.336 Hz. This value compares well to the extracted value computed by ABAQUS.

The mid-point deflection of the test section and the Von Mises stress at the end of the test section were also computed in ABAQUS. The table below lists pertinent information.

It can be seen that the values for mid-point deflection of the test section computed by the ABAQUS FEM code are within 6.0 percent of the solution computed in chapter 2. The predicted Von Mises stress values computed in ABAQUS are within 5.0 percent of the differential equation solution.

	ABAQUS	DIFFERENTIAL EQUATION
MID-POINT DEFLECTION 8 FOOT	1.68 INCHES	1.56 INCHES
VON MISES STRESS 8 FOOT	122,000 PSI	124,596 PSI
MID-POINT DEFLECTION 5 FOOT	1.01 INCHES	0.95 INCHES
VON MISES STRESS 5 FOOT	124,000 PSI	129,885 PSI

4.5 VIBRATION CONSIDERATIONS

The first 50 modes of vibration for the test apparatus are below 10 Hz. These modes include at least the third mode of vibration for each of the major components of the test apparatus. Vibration modes of higher order are considered to have energy levels sufficiently low so that the transfer of vibration to and from the test section can be neglected.

The predicted excitation caused by the vortex shedding is considered to be higher than 10 Hz so that resonant vibrations are unlikely to occur. To insure that the vertical struts and support cables do not contribute to vibration of the test section, drag/strut fairings will be placed on all of these items to reduce drag and vortex shedding.

It can be seen from this chapter that the stress and deflection data presented in chapter 2, agree well with results obtained from ABAQUS, a finite element code. This fact gives greater confidence that the design of the test apparatus is correct. The next phase of the design process will be an assessment of specific mechanical operations such as the tensioning system, rotation system, and instrumentation system.

CHAPTER 5: SUMMARY AND CONCLUSIONS

Data have been correlated and compared from previous experiments that attempted to measure the drag coefficients of wire conduits. These experiments were all performed by towing sections of cable while measuring the tow point tension and the tow angle. With this information, it is possible to calculate the hydrodynamic drag coefficients. It is shown in this work that the uncertainty of these drag coefficients at small angles of attack is on the order of 400 to 500 percent. As a result of the inaccuracies of the critical angle experiments and the application of critical angle data to non-critical angle configurations, an apparatus that measures the normal and tangential drag forces was developed.

The design of the two-point drag apparatus was presented in three succinct steps. A method was developed for stiffening the flexible cable so that the catenary is less than 2 percent of its total length. An instrumentation method was developed so that the normal and tangential forces could be measured accurately. The remaining conceptual design was completed and a vibration analysis performed.

In an effort to reduce the catenary of the test section, it was decided to run a tensioned stainless steel shaft through the middle of the braided cable. The cable itself does not have the strength to survive the adverse conditions

imposed on it by the test apparatus and the hydrodynamic forces. It is evident after a detailed analysis that both the fixed-end and simply supported end conditions of the test section are capable of reducing the catenary to 2 percent of the overall length. The fixed-end condition has significantly higher stresses at the end points. While this is disadvantageous when considering stress, it proves beneficial when considering the mounting of the strain transducers.

The mechanical design of the strain transducers was also presented. Important design criteria for each case were based on linear and uniform strain contours and the percentage of strain in the principal directions. A three-dimensional finite element model of the fixed-end transducer was created to aid in its design. This model not only predicts stress levels in the cross section, but it also shows stress contours that are smooth in all principal directions. Designing the cross sectional area of the fixed end transducer in the form of a rectangle and making its height-to-width ratio 4.0 to 1.0 makes possible accurate measurement of the hydrodynamic loading.

The adequacy of the drag apparatus when considering component vibration was also determined. The first 50 modes of vibration for the test apparatus were below 10 Hz. These modes include at least the third harmonic of each of the major components of the apparatus. The predicted excitation caused

by vortex shedding is considered to be much higher than 10 Hz so that resonant vibrations are unlikely to occur.

A revolutionary design of a two-point attachment apparatus for the measurement of normal and tangential drag coefficients has been presented. This apparatus is capable of accurately measuring the hydrodynamic drag coefficients of flexible cable at various angles of attack and at numerous speeds. The experimental method will be beneficial for the development of computer codes that attempt to predict dynamic behavior of flexible cables in a marine environment.

REFERENCES

1. L. Pode, "An Experimental Investigation of the Hydrodynamic Forces on Stranded Cables," Report 13, David Taylor Model Basin, Washington, DC, 1950.
2. F. Puryear and S. Gay, "Hydrodynamic Loading of Six Configurations of a Towed Flexible Conduit," Report 509-H-01, Naval Ship Research and Development Center, Bethesda, MD, December 1972. [Available to authorized requesters only.]
3. J. Diggs, "Hydrodynamic Characterization of Various Towed Array Towcables," Technical Report 128, Naval Ship Research and Development Center, Bethesda, MD, August 1974. [Available to authorized requesters only.]
4. R. Holler, "Drag Measurements of Long Cables in the Ocean," Report NADC-84086-30, Naval Air Development Center, Warminster, PA, March 1984.
5. J. Babb, S. Hassan, and L. Labrecque, "Normal and Tangential Drag Coefficients for Spiral Wound Flexible Hoses," Technical Memorandum 85-2018, Naval Underwater Systems Center, Newport, RI, April 1985. [Available to authorized requesters only.]
6. J. Milburn, J. Babb, and J. McGrath, "Video Measurement of Equilibrium Tow Angles of Flexible Conduits/Cables," Technical Memorandum 89-2074, Naval Underwater Systems Center, Newport, RI, August 1989. [Available to authorized requesters only.]
7. L. Pode, "Tables for Computing the Equilibrium Configuration of a Flexible Cable in a Uniform Stream," Technical Report 687, David Taylor Model Basin, Washington, DC, 1951.
8. S. Kline and F. McClintock, "Describing Uncertainties in Single-Sample Experiments," Department of Mechanical Engineering, Stanford University, Stanford, CA, 1985.
9. W. Boyce and R. DiPrima, Elementary Differential Equations, John Wiley and Sons, New York, 1977.
10. F. Beer and E. Johnston, Mechanics of Materials, McGraw-Hill, New York, 1981.
11. D. Brown, "Langley Sea Water Tow Tank Facility: Description and Operation," Technical Document 6392, Naval Underwater Systems Center, Newport, RI, June 1985. [Available to authorized requesters only.]

REFERENCES (Cont'd)

12. R. Binder, Fluid Mechanics, Prentice-Hall, Englewood Cliffs, NJ, 1973.
13. M. Every, "A Brief Survey of the Steady Drag Data Available for Application to Unfaired Umbilical Cables," Report 1715, British Hydromechanics Research Association, Bedford, UK, June 1981.
14. C. Perry and H. Lissner, The Strain Gage Primer, McGraw-Hill, New York, 1962.
15. S. Dexter, Handbook of Oceanographic Engineering Materials, John Wiley and Sons, New York, 1979.
16. Hibbitt, Karlson, and Sorenson, "Application Manual for ABAQUS Finite Element Code, Version, 4.8," HKS Inc., 1989.
17. W. Thomson, Theory of Vibrations with Applications, Prentice-Hall, Englewood Cliffs, NJ, 1988.
18. F. White, Fluid Mechanics, McGraw-Hill, New York, 1979.

BIBLIOGRAPHY

- Abkowitz, M., "Towed Bodies," Journal of Mechanical Engineering Science, vol. 14, no. 7, 1972.
- Ackroyd, J., "On the Analysis of Turbulent Boundary Layers on Slender Cylinders," Journal of Fluid Engineering, vol. 104, June 1982.
- Babb, J., S. Hassan, and L. Labrecque, "Normal and Tangential Drag Coefficients for Spiral Wound Flexible Hoses," Technical Memorandum 85-2018, Naval Underwater Systems Center, Newport, RI, April 1985. [Available to authorized requesters only.]
- Batill, S., R. Nelson, and J. Nebres, "An Experimental Investigation of the Flow Around Yawed Stranded Cables," Department of Aerospace and Mechanical Engineering, University of Notre Dame, Notre Dame, IN, November 1989.
- Beer, F., and E. Johnston, Mechanics of Materials, McGraw-Hill, New York, 1981.
- Binder, R., Fluid Mechanics, Prentice-Hall, Englewood Cliffs, NJ, 1973.
- Boyce, W., and R. DiPrima, Elementary Differential Equations, John Wiley and Sons, New York, 1977.
- Brown, D., "Langley Sea Water Tow Tank Facility: Description and Operation," Technical Document 6392, Naval Underwater Systems Center, Newport, RI, June 1985. [Available to authorized requesters only.]
- Celik, I., V. Patel, and L. Landweber, "Calculation of the Mean Flow Past Circular Cylinders by Viscous-Inviscid Interaction," Transactions of the ASME, vol. 107, June 1985.
- Dexter, S., Handbook of Oceanographic Engineering Materials, John Wiley and Sons, New York, 1979.
- Diggs, J., "Hydrodynamic Characterization of Various Towed Array Towcables," Technical Report 128, Naval Ship Research and Development Center, Bethesda, MD, August 1974. [Available to authorized requesters only.]
- Every, M., "A Brief Survey of the Steady Drag Data Available for Application to Unfaired Umbilical Cables," Report 1715, British Hydromechanics Research Association, Bedford, UK, June 1981.

BIBLIOGRAPHY (Cont'd)

- Folb, R., and J. Nelligan, "Hydrodynamic Loading on Armored Towcables," Report DTNSRDC-82/116, David Taylor Naval Ship Research And Development Center, Bethesda, MD, February 1983.
- Hassan, S., and L. Labrecque, "Flexible Hose Breaking Strength Over Existing and Modified Shutter Lips," Technical Memorandum 85-2031, Naval Underwater Systems Center, Newport, RI, 20 May 1985. [Available to authorized requesters only.]
- Hibbitt, Karlson, and Sorenson, "Application Manual for ABAQUS Finite Element Code, Version, 4.8," HKS Inc., 1989.
- Holler, R., "Drag Measurements of Long Cables in the Ocean," Report NADC-84086-30, Naval Air Development Center, Warminster, PA, March 1984.
- Kennedy, Robert M., "Normal and Tangential Hydrodynamic Drag of Very Thin Cylinders in Near Axial Flow," Technical Report 6811, Naval Underwater Systems Center, New London, CT, January 1983. [Available to authorized requesters only.]
- Kennedy, R., and E. Strahan, "A Comparison of Recent Measurements of Boundary Layers on Cylinders in Axial Flow," Technical Memorandum 833001, Naval Underwater Systems Center, AUTECH Detachment, West Palm Beach, FL, April 1983. [Available to authorized requesters only.]
- Kline, S., "The Purposes of Uncertainty Analysis," Journal of Fluids Engineering, vol. 107, June 1985.
- Kline, S., and F. McClintock, "Describing Uncertainties in Single-Sample Experiments," Department of Mechanical Engineering, Stanford University, Stanford, CA, 1985.
- Knutson, R., and K. Eisenberg, "At-Sea Hydrodynamic Evaluation of Bare Double-Armored Tow Cables," Report DTRC-91/007, David Taylor Research Center, Bethesda, MD, July 1991.
- Lueptow, R., P. Leehey, and T. Stellingner, "The Thick Turbulent Layer on a Cylinder: Mean and Fluctuating Velocities," Physics of Fluids A, vol. 28, no. 12, December 1985.
- Milburn, J., J. Babb, and J. McGrath, "Video Measurement of Equilibrium Tow Angles of Flexible Conduits/Cables," Technical Memorandum 89-2074, Naval Underwater Systems Center, Newport, RI, August 1989. [Available to authorized requesters only.]

BIBLIOGRAPHY (Cont'd)

- Perry, C., and H. Lissner, The Strain Gage Primer, McGraw-Hill, New York, 1962.
- Pode, L., "An Experimental Investigation of the Hydrodynamic Forces on Stranded Cables," Report 13, David Taylor Model Basin, Washington, DC, 1960.
- Pode, L., "Tables for Computing the Equilibrium Configuration of a Flexible Cable in a Uniform Stream," Technical Report 687, David Taylor Model Basin, Washington, DC, 1951.
- Puryear, F., and S. Gay, "Hydrodynamic Loading of Six Configurations of a Towed Flexible Conduit," Report 509-H-01, Naval Ship Research and Development Center, Bethesda, MD, December 1972.
- Roark, R., and W. Young, Formulas for Stress and Strain, McGraw-Hill, New York, 1975.
- Robert, M., and L. Keer, "Stiffness of an Elastic Circular Cylinder of Finite Length," Transactions of the ASME, vol. 55, September 1988.
- Taylor, G., "Analysis of the Swimming of Long and Narrow Animals," Proceedings of the Royal Society, vol. 214, February 1952.
- Thomson, W., Theory of Vibrations with Applications, Prentice-Hall, Englewood Cliffs, NJ, 1988.
- Whicker, L., "An Analysis of Axisymmetric Turbulent Flow Past a Long Cylinder," Transactions of the ASME, March 1972.
- White, F., Fluid Mechanics, McGraw-Hill, New York, 1979.

INITIAL DISTRIBUTION LIST

Addressee	No. of Copies
Defense Technical Information Center	2
Center for Naval Analyses	1